

# Geochemical evidence for interaction between oceanic crust and lithospheric mantle in the origin of Cenozoic continental basalts in east-central China

Jun-Jun Zhang, Yong-Fei Zheng\*, Zi-Fu Zhao

CAS Key Laboratory of Crust–Mantle Materials and Environments, School of Earth and Space Sciences, University of Science and Technology of China, Hefei 230026, China

## ARTICLE INFO

### Article history:

Received 13 August 2008

Accepted 22 January 2009

Available online 30 January 2009

### Keywords:

Continental basalt

Subcontinental lithospheric mantle

Oceanic crust

Slab melt

Pyroxenite

## ABSTRACT

Cenozoic continental basalts from east-central China have been analysed for whole-rock major and trace elements, Sr–Nd–Hf isotopes, and mineral O isotopes. The basalts are alkalic to tholeiitic in composition, but are dominantly alkalic. They are characterized by OIB-like patterns of trace element distribution, with no depletion in Nb and Ta but with negative Pb anomalies on primitive mantle normalized diagrams. In addition, they have high Fe/Mn ratios and subchondritic Nb/Ta ratios. Sr–Nd–Hf isotope compositions indicate predominant contributions from young subcontinental lithospheric mantle (SCLM). Some phenocrysts of clinopyroxene and olivine have lower O isotope ratios than normal upper mantle, suggesting involvement of low  $\delta^{18}\text{O}$  melts derived from dehydrated oceanic basalt that experienced high-T seawater-hydrothermal alteration during MORB-type magma eruption. Such low  $\delta^{18}\text{O}$  melts are unlikely to be transported through the convective asthenosphere because of its rapid O isotope homogenization, but likely to directly metasomatize the overlying peridotite to form pyroxenite. Oxygen isotope disequilibrium between olivine and clinopyroxene suggests a maximum timescale of <1 ka for melting, transport and eruption during basaltic magmatism. Therefore, we propose a model of oceanic crust–lithospheric mantle interaction for petrogenesis of the continental basalts, in that they were principally derived from near-solidus partial melting of pyroxenites in the juvenile SCLM. Low-angle subduction of the oceanic crust beneath the continental lithosphere during the Early Mesozoic would have not only delaminated the ancient SCLM into the asthenosphere to result in the mantle heterogeneity, but also transform the overlying mantle wedge to the juvenile SCLM beneath the thinned ancient SCLM. Partial melting of the dehydrated oceanic metabasalt and metasediment during the Late Mesozoic would generate adakitic and felsic melts, respectively, metasomatize the overlying juvenile SCLM peridotite to form isotopically depleted silica-deficient to enriched silica-excess pyroxenites. As a result, SCLM beneath the eastern China was stratified in the Cenozoic, with the juvenile SCLM underlying the ancient SCLM but overlying the pyroxenites. Lithosphere rifting during the Cenozoic would cause the melting of the pyroxenites, giving rise to the alkalic to tholeiitic basalts. Therefore, the Cenozoic continental basalts provide the petrological record of melt–peridotite reactions in response to the asthenosphere–lithosphere interaction during the Mesozoic thinning of continental lithosphere.

© 2009 Elsevier B.V. All rights reserved.

## 1. Introduction

Many, if not all, continental basalts are characterized by oceanic island basalt (OIB)-like trace element signatures and moderately depleted Nd and Sr isotope compositions. Interpretation of their origin, however, is diverse and often controversial. It is usually attributed to one of the following processes: (1) mantle plumes (Burke and Wilson, 1976; Richards et al., 1989; Campbell and Griffiths, 1990), (2) extension of continental lithosphere (McKenzie and Bickle, 1988; White and McKenzie, 1989), or (3) melting of wet subcontinental lithospheric

mantle (Gallagher and Hawkesworth, 1992). Thus, mantle plumes, the upper asthenosphere, oceanic and continental lithosphere (on their own or in combination) have all been considered as possible sources for continental basaltic magmatism (e.g., Anderson, 1994; White and McKenzie, 1995; Gibson et al., 1996; Barry et al., 2003; Anderson, 2005; Lustrino, 2005; Silver et al., 2006). Since basalts in continental settings are less abundant than those in oceanic settings, their origin is less clearly defined than those in oceanic settings (e.g., Zindler and Hart, 1986; Hofmann, 1997). However, insight into the origin of continental basalts is of fundamental importance to understanding of lithosphere–asthenosphere interaction within the framework of chemical geodynamics.

One notable occurrence of Cenozoic continental basalts occurs in the eastern part of China. These basalts share trace element and Nd–Sr isotope characteristics with continental basalts elsewhere in the world. A number of geological and geochemical studies have been carried out

\* Corresponding author.

E-mail address: [yfzheng@ustc.edu.cn](mailto:yfzheng@ustc.edu.cn) (Y.-F. Zheng).

on these basalts in the past two decades (e.g., Zhou and Armstrong, 1982; Peng et al., 1986; Dostal et al., 1988; Zhi et al., 1990; Basu et al., 1991; Fan and Hooper, 1991; Chung et al., 1994; Liu et al., 1994; Qi et al., 1994; Flower et al., 1998; Smith, 1998; Chung, 1999; Zou et al., 2000; Xu et al., 2005; Niu, 2005; Tang et al., 2006; Chen et al., 2007). These studies have suggested the existence of distinct mantle components (including both enriched and depleted mantle), but mantle processes responsible for the Cenozoic basalts are still unclear. Geodynamically, petrogenesis of the Cenozoic basalts was originally interpreted in terms of hotspots (e.g., Deng et al., 1998, 2004). Alternatively, it has been suggested that the basaltic volcanism may be related to large scale interaction between Asia, the Pacific and Indian Plates (e.g., Smith, 1998; Tang et al., 2006), leading to melt generation in far backarc extension settings (e.g., Song et al., 1990; Zou et al., 2000).

Because the depleted isotope signature predominates in these Cenozoic basalts from China, it has been commonly hypothesized that they were derived from partial melting of the convective asthenosphere or lithosphere–asthenosphere interaction (e.g., Zou et al., 2000; Xu et al., 2005; Tang et al., 2006). Such a hypothesis presumes that the depleted mantle source is the asthenosphere. These models however do not consider prior enrichment that may have transformed the asthenosphere to the juvenile subcontinental lithospheric mantle (SCLM). Furthermore, they cannot explain how a MORB-like trace element fingerprint from the asthenosphere was transformed into an OIB-like trace element signature as observed in the continental basalts. On the other hand, these existing models attributed the enriched isotope signature in some of the basalts to involvement of craton SCLM, without distinction between ancient and juvenile SCLMs in magma sources. Alternatively, Niu (2005) proposed the transformation of lithospheric mantle to asthenospheric mantle by adding dehydrated fluids. However, the involvement of aqueous fluids in mantle metasomatism would result in basalts depleted in high field strength elements (HFSE) as commonly observed in oceanic arc basalts (Hawkesworth et al., 1991; Tatsumi and Eggins, 1995). These arc-like trace element signatures are, however, not observed in the Cenozoic basalts of eastern China.

The North China Block and the South China Block have been assembled into a unified continent since the Triassic collision along the Qinling–Dabie–Sulu orogenic belt (e.g., Cong, 1996; Li et al., 1999; Zheng, 2008). No significant differences are expected in petrotectonic evolution between the two blocks during the Cenozoic and even back to the Cretaceous and Jurassic. Thus, Cenozoic continental basalts from east-central China are also of great interest in understanding the mechanism and geodynamics of craton SCLM thinning in North China during the Phanerozoic (e.g., Menzies et al., 1993; Griffin et al., 1998; Fan et al., 2000; Xu, 2001; Zheng et al., 2001; Gao et al., 2002; Wu et al., 2003; Rudnick et al., 2004; Menzies et al., 2007). Geotectonically, the North China Block is surrounded by three subduction zones that formed during the Phanerozoic: the Paleozoic subduction of the Siberian Plate along the northern edge, the Early Mesozoic subduction of the South China Block along the southern edge, and the Mesozoic–Cenozoic subduction of the Pacific Plate along the eastern edge. Therefore, the physical and chemical effects of subduction on the craton SCLM thinning must be taken into account when interpreting petrogenesis of Mesozoic and Cenozoic igneous rocks in the North China Block and its adjacent areas. The OIB-like characteristics of trace elements and radiogenic isotopes also occur in Cenozoic continental basalts in the North China Block (e.g., Zou et al., 2000; Xu et al., 2005; Tang et al., 2006), suggesting that the SCLM thinning likely took place during the Mesozoic or earlier rather than the Cenozoic. Thus, it is intriguing how pre-Cenozoic subduction led to thinning of the craton SCLM in the North China Block, leaving space for the formation of juvenile SCLM for the continental basaltic magmatism.

In this study we aim to answer the following eight questions. (1) Can the juvenile SCLM generate the isotopically depleted signature in continental basalts like that from the asthenosphere? (2) Can

pyroxenites melt in the SCLM to generate different compositions of continental basalts? (3) Can compositional differences between the different compositions of continental basalts be caused by differences in the nature of melts that metasomatized SCLM peridotite? (4) Can different materials on subducted oceanic crust melt to generate different slab melts for formation of different pyroxenites? (5) Can the craton SCLM be delaminated by low-angle subduction of oceanic lithosphere? (6) Can the low-angle subduction transform the mantle wedge to the juvenile SCLM beneath the thinned craton SCLM? (7) Can the craton SCLM be delaminated into the asthenosphere causing mantle heterogeneity? (8) Can part of the craton SCLM survive as a residual layer between the continental crust and the juvenile SCLM in the Cenozoic?

In this paper, we present an integrated study of whole-rock major and trace elements, Sr–Nd–Hf isotopes, and phenocryst O isotopes for Cenozoic continental basalts from eastern Anhui (Wandong) and northern Jiangsu (Subei) in east-central China. The results provide insights not only into the geochemical compositions of the shallow upper mantle in east-central China, but also into the origin of continental basalts from variable contributions from juvenile SCLM due to involvement of subducted oceanic crust. In particular, pyroxenites are considered as the source of continental basalts. Finally, we propose a model of oceanic crust–lithospheric mantle interaction for petrogenesis of the continental basalts in which the mantle source formed by adding small amounts of partial melts from the dehydrated oceanic crust to the young lithospheric mantle.

## 2. Geological setting

Along the eastern Asian continental margin, Cenozoic extensional basins and associated predominantly basaltic volcanic rocks are extensively developed over 4000 km from Siberia to southeastern China (Zhou and Armstrong, 1982; Fan and Hooper, 1991; Chung et al., 1994). In eastern China within the eastern edge of Eurasian continent, Cenozoic basalts are widely distributed along the coastal provinces and adjacent offshore shelf from the northernmost in Heilongjiang province to the southernmost in Hainan island, and constitute the eastern China volcanic belt. A close spatial relationship between Paleogene basalts and sedimentary basins in eastern China suggests that Cenozoic basaltic magmatism was probably associated with extension and thinning of the lithosphere along the eastern edge of the Eurasian continent (Ma and Wu, 1987; Watson et al., 1987; Tian, 1990). Neogene basalts, however, are not confined to basins but occur also on craton margins.

The east-central part of China is characterized by the Dabie–Sulu orogenic belt (insert in Fig. 1), which is a Triassic collision zone between the North China Block and the South China Block (Li et al., 1999; Zheng et al., 2003, 2005). It is truncated at its eastern end by the Tanlu fault, which offsets the ultrahigh-pressure (UHP) Dabie orogen by a minimum of 530 km northward to the Shandong peninsula where it occurs as the Sulu orogen. Zircon U–Pb dating for eclogite-facies metamorphic rocks consistently gives Middle Triassic ages of 240 to 225 Ma for UHP metamorphic event (Liu et al., 2006a,b; Wu et al., 2006). Zircon U–Pb dates for mafic and felsic protoliths of most Dabie–Sulu UHP metaigneous rocks (Zheng et al., 2004; Tang et al., 2008a,b) and low-grade counterparts (Huang et al., 2006; Wu et al., 2007; Zheng et al., 2007) range from 700 to 800 Ma, with a cluster around 740 to 780 Ma. These ages are interpreted to date rifting magmatism in response to breakup of the supercontinent Rodinia during middle Neoproterozoic along the northern margin of the South China Block (Zheng et al., 2004, 2006, 2007).

The samples used in this study were collected from the north-eastern edge of the South China Block, east of the Tanlu fault, and the southern margin of the Subei basin (Fig. 1). Geographically, they are located in eastern Anhui (Wandong) and northern Jiangsu (Subei). These samples are called the Wan–Su basalts in this paper. The well-known Cenozoic basalts at Nushan and Panshishan are located

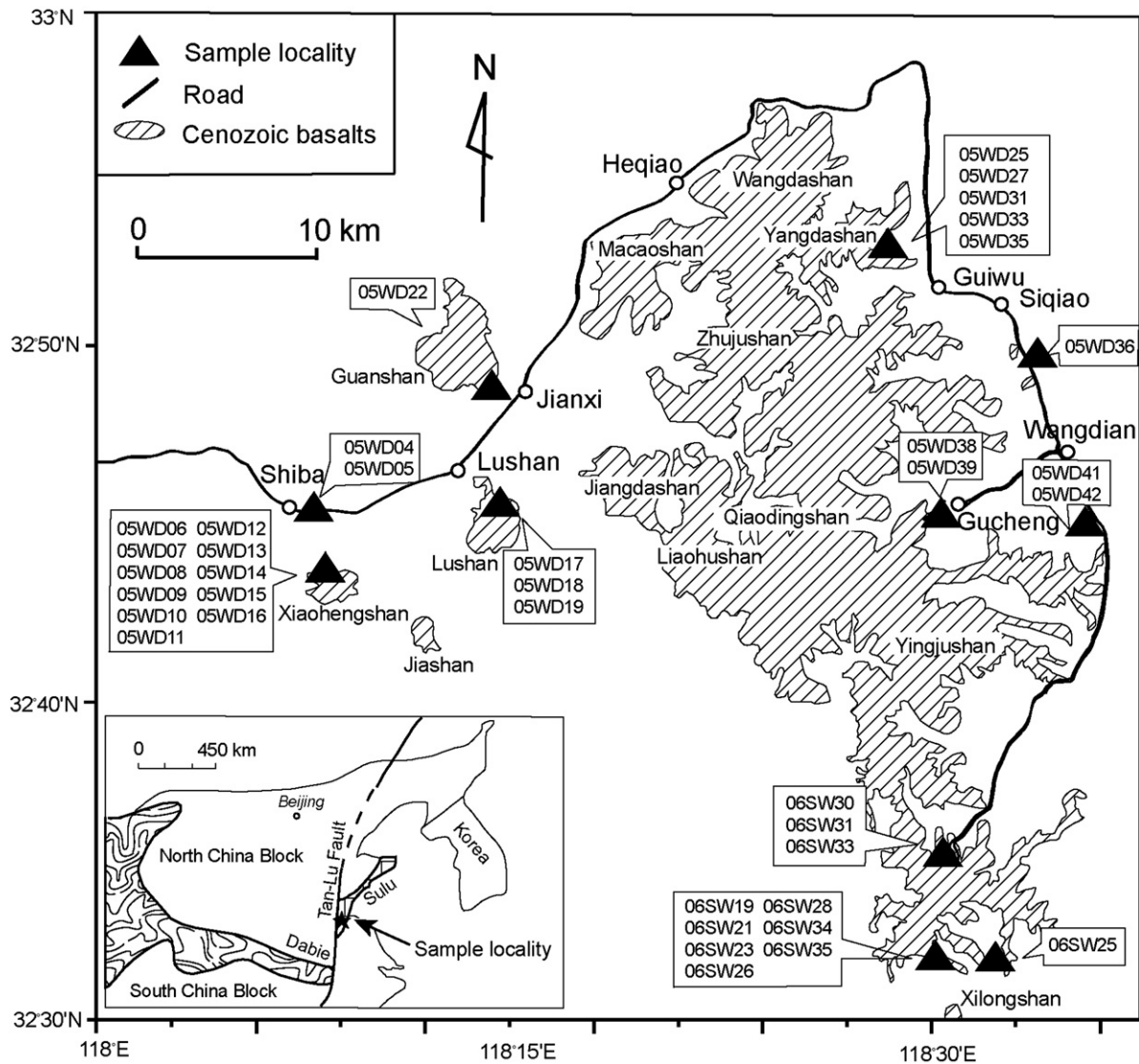


**Fig. 1.** Distribution of the Cenozoic basalts in Wan-Su (eastern Anhui and northern Jiangsu) volcanic field and sampling localities. Note that the North China Block is cut by Tan-Lu fault zone (TLFZ).

northwest and southeast of this region, respectively. The Wan-Su basalts occur as lava flows of central fissure type with an outcrop area over 1000 km<sup>2</sup>. The Subei basin is filled mainly by thick non-marine sediments (shales and sandstones) of Late Triassic to Pleistocene age and by basaltic rocks of Paleocene to Pleistocene age (Chen and Peng, 1988; Dostal et al., 1988; Zhou et al., 1988).

### 3. Samples and petrography

Thirty-eight samples of Cenozoic basalts were collected from various volcanic cones: Xiaohengshan, Lushan and Guanshan in Mingguang City, the eastern edge of Anhui Province, and Yangdashan, Siquiao, Wangdian, Gucheng and Changshan in Huai'an City, the northern part of Jiangsu Province. The localities and descriptions of these samples are listed in online Table S1. According to stratigraphic and paleontological constraints, Cenozoic basalts were erupted from these volcanic cones in two magmatic cycles: one in the Miocene and the other in the Pliocene (Anhui BGMR, 1978). Both alkalic and tholeiitic basalts occur in the Wan-Su area, without temporal distinction in eruption sequence between them in the field. Whole-rock K-Ar dating yielded Miocene ages of  $15.4 \pm 0.4$  Ma and  $16.5 \pm 0.3$  Ma for the alkali basalt at Qingmingshan (Chen and Peng, 1988). Detailed sampling locations are shown in Fig. 1. Phenocryst O isotope

analysis was carried out for all thirty-six samples; twenty-seven samples were analysed for whole-rock major and trace elements as well as Sr-Nd-Hf isotopes.

The basalts are gray, dark gray or dark in colour, with porphyritic texture, and massive, vesicular or amygdaloidal structure. The alkali basalt has olivine (<8%), clinopyroxene (5–10%) and plagioclase (3–10%) as phenocrysts. The tholeiitic basalt has olivine (<6%), clinopyroxene (5–15%) and plagioclase (5–12%) as phenocrysts. Olivine phenocrysts are subhedral to xenomorphic in shape. Some of them were partially altered to low-temperature iddingsite, which is characterized by its occurrence in the periphery and fractures of olivine phenocrysts (Goff, 1996; Caroff et al., 2000). Clinopyroxene phenocrysts are euhedral to subhedral, and some have compositional zonation. The groundmass is microcrystalline and consists of plagioclase, clinopyroxene, olivine and Fe-Ti oxides in addition to basaltic glass.

### 4. Analytical methods

The samples were sawed into slabs and the central parts were used for whole-rock analyses. Specimens were crushed in a steel mortar and ground in a steel mill to powders of ~200 mesh. Mineral grains were separated by magnetic and heavy-liquid techniques, and then handpicked from sieve fractions under a binocular microscope.

**Table 1**  
Major element compositions of Cenozoic basalts in Wan–Su.

Lithology sample	Alkali basal														
	05WD06	05WD08	05WD09	05WD15	05WD16	05WD31	05WD33	06WD38	05WD42	06SW19	06SW21	06SW23	06SW30	06SW31	06SW34
<i>Major oxides (%)</i>															
SiO <sub>2</sub>	46.31	45.94	48.31	46.96	45.34	43.04	42.48	45.98	47.73	43.66	40.57	41.04	46.08	46.83	47.17
TiO <sub>2</sub>	2.51	2.50	2.34	2.53	2.45	2.76	2.77	2.58	2.06	2.52	2.45	2.36	2.12	2.17	1.78
Al <sub>2</sub> O <sub>3</sub>	13.03	12.94	13.43	13.39	12.61	12.57	12.44	13.09	13.06	12.04	11.30	11.17	12.69	13.02	14.53
TFe <sub>2</sub> O <sub>3</sub>	11.68	12.81	11.65	12.99	12.32	13.25	13.74	13.33	11.92	14.50	14.16	13.68	12.60	12.62	14.40
FeO	3.52	5.78	3.37	4.40	7.90	5.52	4.10								
MnO	0.13	0.15	0.12	0.15	0.16	0.16	0.16	0.16	0.15	0.16	0.18	0.17	0.15	0.15	0.16
MgO	6.96	8.38	6.10	6.03	8.88	9.40	7.76	6.79	6.52	7.25	12.10	12.00	7.06	7.66	6.67
CaO	9.24	8.88	8.78	8.89	8.99	8.87	9.25	9.09	10.64	9.54	8.96	9.24	10.86	10.05	8.75
Na <sub>2</sub> O	4.44	4.40	3.86	4.11	3.45	6.54	5.86	3.68	3.24	4.90	4.77	4.15	3.48	3.61	3.96
K <sub>2</sub> O	2.12	2.02	1.92	2.15	2.13	0.96	1.04	2.05	1.77	1.28	1.75	1.71	1.66	1.70	1.19
P <sub>2</sub> O <sub>5</sub>	0.81	0.80	0.68	0.86	0.75	0.84	1.10	0.81	0.51	1.00	1.05	1.04	0.53	0.55	0.57
LOI	2.43	1.84	2.42	1.52	2.63	1.82	3.10	1.78	2.57	2.93	2.68	3.22	2.93	1.88	0.77
Total	99.66	100.66	99.61	99.58	99.71	100.21	99.70	99.33	100.17	99.79	99.97	99.78	100.16	100.24	99.95

Whole-rock major elements were determined on fused glass discs using a Phillips PW1400 X-ray fluorescence spectrometer (XRF) at the Institute of Geology and Geophysics (IGG), Chinese Academy of Sciences, Beijing. Analytical precision was better than 5%, estimated from repeated analyses of two standards (andesite GSR-2 and basalt GSR-3). A few samples were reanalyzed by ICP-MS after dissolution at China University of Geosciences in Wuhan for the purpose of examining the accuracy of Fe/Mn ratios (Liu et al., 2008), yielding the same results as the previous ones, within analytical uncertainties.

Trace element abundances were measured on an Element 1 ICP-MS at IGG after complete dissolution. Powders (~40 mg) were dissolved in distilled HF + HNO<sub>3</sub> in 15 ml Saville Teflon screw-cap beakers at 190 °C for 5 days, dried and then diluted to 50 ml for analysis. Indium was used as an internal standard to correct for matrix effects and instrument drift. Three standards (granite GSR-1, andesite GSR-2, and basalt GSR-3) were used to monitor the analytical quality. Precision for all trace elements is estimated to be ± 5%, and accuracy is better than ± 5% for most trace elements.

Rb–Sr and Sm–Nd isotopic analyses were performed on a Finnigan MAT-262 thermal ionization mass spectrometer (TIMS) at IGG. The powders (~100 mg) were weighed, spiked with mixed isotope tracers and dissolved in Teflon capsules with HF + HClO<sub>4</sub> at 120 °C for 7 days. Separations of Rb, Sr and light REE (LREE) were carried out with a cation-exchange column (packed with AG50Wx8). Sm and Nd were further purified using a second cation-exchange column (packed with AG50Wx12). Total procedural blanks were <200 pg for Sr and <50 pg for Nd. The mass fractionation corrections for Sr and Nd isotopic ratios were based on <sup>86</sup>Sr/<sup>88</sup>Sr of 0.1194 and <sup>146</sup>Nd/<sup>144</sup>Nd of 0.7219, respectively. During our analyses, measured <sup>87</sup>Sr/<sup>86</sup>Sr ratios for standard NBS987 are 0.710253 ± 0.000010, and measured <sup>143</sup>Nd/<sup>144</sup>Nd ratios for the La Jolla standard are 0.511862 ± 0.000009 (in 2σ uncertainty for 28 analyses). Further details on the analytical techniques are given in Chen et al. (2000, 2002b). Single-stage Nd model ages (T<sub>DM1</sub>) were calculated relative to the depleted mantle reservoir with <sup>143</sup>Nd/<sup>144</sup>Nd and <sup>147</sup>Sm/<sup>144</sup>Nd ratios of 0.513151 and 0.2137, respectively (DePaolo, 1988).

Lu–Hf isotopes were analysed on a Neptune MC-ICP-MS at IGG. The powders (~100 mg) were dissolved in Teflon capsules with HF + HClO<sub>4</sub> at 120 °C for 7 days, dried and then dissolved with 3 N HCl. Hafnium could be effectively separated from major and rare earth elements as well as the interference elements with an anion-exchange column (packed with Ln-Spec resin). This modified method is based on the procedures of Muenker et al. (2001) and Li et al. (2005). All were normalized against a <sup>179</sup>Hf/<sup>177</sup>Hf ratio of 0.7325. During our analyses, measured <sup>176</sup>Hf/<sup>177</sup>Hf ratios are 0.282160 ± 0.000011 for standard JMC-475, 0.283087 ± 0.000012 for standard BHVO-2, 0.282754 ± 0.000010 for standard W-2, and 0.282986 ± 0.000009 for standard JB-1 (2σ, n=90). All of them are identical with those reference values within

analytical errors (Le Fevre and Pin, 2001; Kleinhanns et al., 2002; Bizzarro et al., 2003). Single-stage Hf model ages (T<sub>DM1</sub>) were calculated relative to the depleted mantle reservoir with <sup>176</sup>Hf/<sup>177</sup>Hf and <sup>176</sup>Lu/<sup>177</sup>Hf ratios of 0.28325 and 0.0384, respectively (Griffin et al., 2000).

Mineral O isotope analyses were carried out by laser fluorination using a 25 W CO<sub>2</sub> laser MIR-10 at University of Science and Technology of China in Hefei. Grained minerals with weight of about 1.5 mg were reacted with BrF<sub>5</sub> under vacuum. Oxygen gas was obtained and then directly transferred to a Delta XP mass spectrometer for the measurements of <sup>18</sup>O/<sup>16</sup>O and <sup>17</sup>O/<sup>16</sup>O ratios (Zheng et al., 2002). The <sup>18</sup>O/<sup>16</sup>O ratios were reported in the δ<sup>18</sup>O notation relative to the VSMOW standard. The reproducibility is better than ± 0.1‰ (1σ, n=2). Two standards were used during the laser fluorination analyses: (1) δ<sup>18</sup>O = 5.8‰ for garnet UWG-2 (Valley et al., 1995); (2) δ<sup>18</sup>O = 11.11‰ for quartz GBW04409 (Zheng et al., 1998).

## 5. Results

### 5.1. Major elements

Major element results are shown in Table 1. According to the nomenclature of Le Bas et al. (1986), the Wan–Su basalts are tephrite, basanite, trachybasalt, basalt and basaltic andesite (Fig. 2). In terms

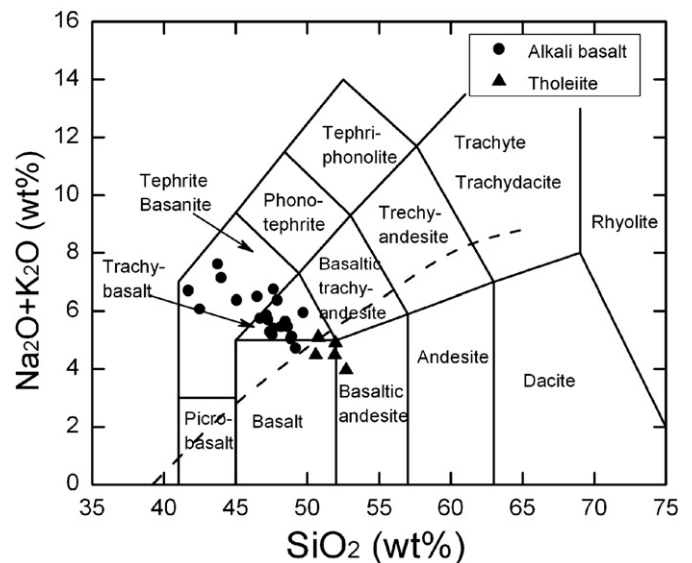


**Fig. 2.** Total alkalis vs. SiO<sub>2</sub> diagram for Cenozoic basalts in Wan–Su (the framework is after Le Bas et al., 1986).

					Tholeiite							Standards			
06SW35	05WD11	05WD18	05WD22	06SW25	05WD05	05WD36	05WD39	05WD41	06SW26	06SW28	06SW33	GSR-2	GSR-3		
46.95	47.17	47.49	46.16	47.31	50.88	49.68	51.84	48.73	48.28	49.86	50.08	60.72	60.66	44.40	44.30
1.63	2.54	2.62	2.19	1.61	2.08	2.10	1.71	2.13	2.35	1.50	1.68	0.53	0.53	2.34	2.34
13.77	13.52	12.83	13.43	14.13	14.25	14.99	14.24	13.49	12.93	14.51	15.25	16.33	16.32	13.73	13.72
13.81	13.16	12.52	11.48	14.18	11.81	12.98	11.62	12.22	12.81	11.99	11.94	5.11	5.13	13.42	13.50
	3.00	3.62	3.67		4.28	1.76	5.56	4.66							
0.17	0.15	0.13	0.13	0.17	0.15	0.15	0.14	0.15	0.15	0.15	0.15	0.08	0.08	0.17	0.17
8.72	5.41	7.48	7.31	6.21	5.60	3.86	6.48	6.06	6.59	6.15	5.69	1.69	1.70	7.77	7.79
8.03	8.99	8.57	8.46	8.59	7.93	7.17	8.12	8.67	9.85	8.70	8.46	5.22	5.22	8.79	8.77
4.15	4.01	3.49	3.02	3.88	3.29	2.63	2.80	2.62	3.64	3.65	3.48	3.89	3.85	3.34	3.44
1.52	1.49	1.84	1.74	1.48	1.52	1.67	1.10	1.71	0.99	1.34	1.56	1.87	1.86	2.31	2.30
0.58	0.91	0.71	0.58	0.66	0.42	0.47	0.31	0.55	0.60	0.31	0.37	0.24	0.24	0.94	0.94
0.03	2.10	2.12	4.91	1.13	1.50	3.68	1.27	3.13	1.80	1.37	0.75	4.55	4.55	2.60	2.60
99.37	99.45	99.80	99.41	99.35	99.43	99.38	99.63	99.46	99.99	99.53	99.41	100.23	100.14	99.81	99.87

of CIPW normative calculations (online Table S2), 20 samples are categorized into alkali basalt and the remaining 7 samples into tholeiite. The alkali basalt has SiO<sub>2</sub> of 40.57 to 48.31%, TiO<sub>2</sub> of 1.61 to 2.77%, MgO of 5.41 to 12.10%, Al<sub>2</sub>O<sub>3</sub> of 11.17 to 14.53%, Mg numbers of 44.88 to 63.47 and Fe/Mn ratios of 69.54 to 87.68 (online Table S3). In contrast, the tholeiite has higher SiO<sub>2</sub> (48.28 to 51.84%) and Al<sub>2</sub>O<sub>3</sub> (12.93 to 15.25%), lower MgO (3.86 to 6.59%), Fe<sub>2</sub>O<sub>3</sub>, CaO and Na<sub>2</sub>O, lower Mg numbers of 37.07 to 52.49, and Fe/Mn ratios of 71.11 to 78.15. When plotted against SiO<sub>2</sub> (Fig. 3), TiO<sub>2</sub>, Fe<sub>2</sub>O<sub>3</sub>t, MgO, CaO and Na<sub>2</sub>O display negative correlations for both the alkalic and tholeiitic basalts, and Al<sub>2</sub>O<sub>3</sub> displays a positive correlation. There are variable LOI values for different samples (Table 1), which are 0.03 to 4.91% for the alkali basalt and 0.75 to 3.68% for the tholeiite.

## 5.2. Trace elements

Table 2 lists rare earth element (REE) and other trace element abundances. The Wan–Su basalts have smooth chondrite-normalized REE patterns similar to those of oceanic island basalts (OIB) with moderate LREE enrichment (Fig. 4a and b). In general, the alkali basalt shows high LREE but low HREE contents (Fig. 4a), with high (La/Yb)<sub>N</sub> ratios of 12.5 to 31.8 (Table S3). The tholeiite has consistently lower REE contents than OIB (Fig. 4b), with low (La/Yb)<sub>N</sub> ratios of 7.07 to 14.4. Both the alkalic and tholeiitic basalts have no significant Eu anomaly, suggesting that plagioclase is not a major fractionating phase.

The alkali basalts show no depletion in Nb and Ta on primitive-mantle normalized multi-element plots but have negative Pb anomalies (Fig. 4c), similar to the pattern for OIB. Although the tholeiites also display no depletion in Nb and Ta, their trace element concentrations are almost consistently lower than those of OIB (Fig. 4d). Except for samples 05WD39 and 06SW28 that show positive Pb anomalies with low U, Nb and Ta contents, all the other samples have negative Pb anomalies, and almost consistent Nb/Ta ratios of 14.49 to 17.37 for the alkali basalt and 15.35 to 16.41 for the tholeiite (Table S3). Except for tholeiite 06SW28 that has an anomalously high Nb/U ratio of 84.7, all the other basalts have Nb/U ratios of 34.2 to 57.2 (Table S3), basically falling within the field of OIB (Nb/U = 47 ± 10; Hofmann et al., 1986). Except for tholeiite 06SW26 with a high U content of 1.05 ppm, the other tholeiites have U contents of 0.26 to 0.78 ppm that are generally lower than those of 0.65 to 2.29 ppm for the alkali basalts (Table 2).

## 5.3. Sr–Nd–Hf isotopes

The Rb–Sr, Sm–Nd and Lu–Hf isotopic compositions of the Wan–Su basalts are shown in Tables 3–5, respectively. The initial Sr, Nd and Hf isotopic compositions were calculated at  $t = 16$  Ma following the K–Ar

dating of Chen and Peng (1988). The alkali basalt has  $I_{Sr}(t)$  values of 0.703271 to 0.704458,  $\epsilon_{Nd}(t)$  values of  $-1.96$  to 6.89, and  $\epsilon_{Hf}(t)$  values of  $-2.75$  to 11.19, with Nd model ages of 293 to 1260 Ma and Hf model ages of 267 to 1013 Ma. In contrast, the tholeiite has  $I_{Sr}(t)$  values of 0.704231 to 0.704995,  $\epsilon_{Nd}(t)$  values of  $-7.67$  to 2.19, and  $\epsilon_{Hf}(t)$  values of  $-5.92$  to 2.15, with Nd model ages of 824 to 1953 Ma and Hf model ages of 730 to 1157 Ma. The alkali basalt is generally more depleted in radiogenic Sr, Nd and Hf isotopes than the tholeiite. Taking the two types of basalt together, there is a negative correlation between the Sr and Nd isotopic ratios (Fig. 5a), but a positive correlation between the Nd and Hf isotope ratios (Fig. 5b) except one tholeiite offset (05WD05). In either case, the Wan–Su basalts were originated from isotopically heterogeneous sources, with contrasting contributions from relatively depleted and enriched components, respectively, for the alkalic and tholeiitic basalts.

## 5.4. Phenocryst O isotopes

Oxygen isotope data for clinopyroxene and olivine phenocrysts from the Wan–Su basalts are presented in Table 6 (13 samples are the alkali basalt, 6 samples are the tholeiite, and the remaining 8 samples are unclassified). Clinopyroxene in the alkali basalt has  $\delta^{18}O$  values of 4.42‰ to 5.50‰, whereas clinopyroxene in the tholeiite has relatively high  $\delta^{18}O$  values of 5.02‰ to 5.70‰. Olivine in the two subtypes of basalts has  $\delta^{18}O$  values of 4.00‰ to 5.91‰. The O isotopes for clinopyroxene and olivine in the 27 basalts are plotted in Fig. 6a and b, respectively. For olivine,  $\delta^{18}O$  values of  $5.2 \pm 0.2\%$  appear to be a good estimate for the oxygen isotope composition of most mantle reservoirs sampled by MORB, hotspot magmas and xenoliths (Eiler et al., 1996). Clinopyroxene  $\delta^{18}O$  values of  $5.6 \pm 0.2\%$  would thus be in equilibrium with olivine assuming an equilibrium fractionation ( $\Delta^{18}O_{Cpx-Ol}$ ) of 0.4‰ estimated from experimental and theoretical considerations at temperatures of 1000 to 1200 °C (Chiba et al., 1989; Zheng, 1993). Clinopyroxene  $\delta^{18}O$  values from the Wan–Su basalts are mostly lower than the normal mantle values of  $5.6 \pm 0.2\%$  (Fig. 6a), with the lowest  $\delta^{18}O$  values of 4.42 to 4.86‰ in the alkali basalt. In contrast, most olivine  $\delta^{18}O$  values approach the normal mantle values of  $5.2 \pm 0.2\%$  (Fig. 6b). Olivine from a few samples of the alkali basalt shows distinctly lower or higher  $\delta^{18}O$  values: 05WD16 and 06SW25 have the lowest values of 4.00‰ and 4.48‰, respectively, and sample 06SW19 has a value of 5.91‰. Taken together, the alkali basalt shows a larger variation in phenocryst  $\delta^{18}O$  values, with lower  $\delta^{18}O$  values, than the tholeiite.

## 6. Discussion

Sr, Nd and Hf isotope compositions in basaltic melts are determined by the nature of the source. This is somewhat similar to

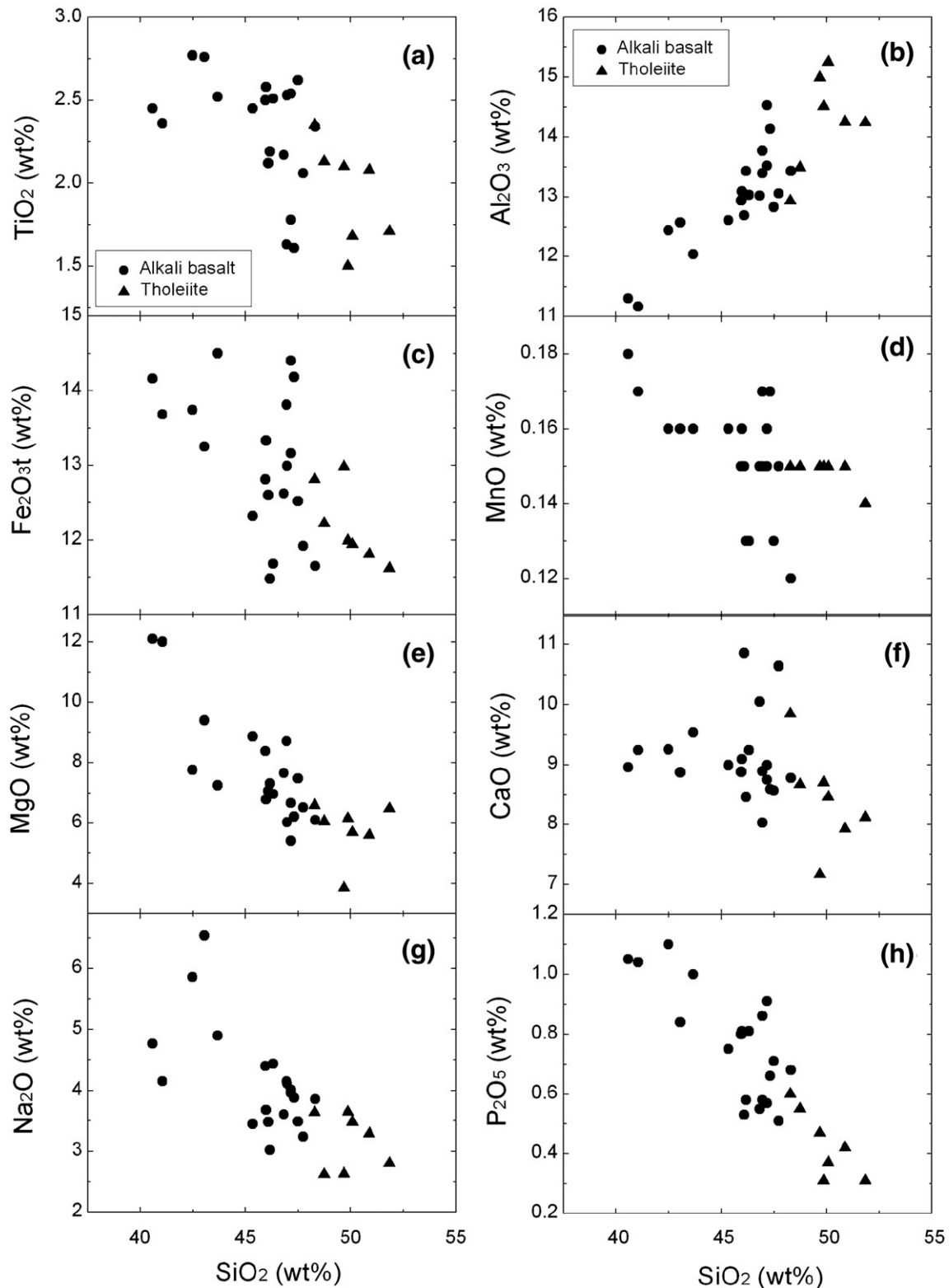


Fig. 3. Variations of  $\text{TiO}_2$ ,  $\text{Al}_2\text{O}_3$ ,  $\text{Fe}_2\text{O}_3\text{t}$ ,  $\text{MnO}$ ,  $\text{MgO}$ ,  $\text{CaO}$ ,  $\text{Na}_2\text{O}$  and  $\text{P}_2\text{O}_5$  versus  $\text{SiO}_2$  for the Wan-Su basalts.

the behaviour of the highly incompatible trace element ratios. Because of the moderately incompatible character of elements Sr, Nd and Hf, however, melt mixing is not as effective in averaging isotope ratios as it is for the highly incompatible trace element ratios. Consequently, basaltic melts extracted from heterogeneous mantle sources may have not recorded the full range of isotopic heterogeneity in their source. Therefore, the chemical and isotopic compositions of continental

basalts are controlled primarily by the mineralogy and geochemical composition of the mantle sources, the extent and depth of partial melting, and shallow processes such as crustal contamination and crystal fractionation. The relative importance of these factors and processes in generating the Wan-Su basalts are discussed below.

It is likely that variations in some element concentrations and isotope compositions could be caused by post-magmatic alteration.

**Table 2**  
Trace element compositions of Cenozoic basalts in Wan-Su.

Lithology sample	Alkali basalt														
	05WD06	05WD08	05WD09	05WD15	05WD16	05WD31	05WD33	06WD38	05WD42	06SW19	06SW21	06SW23	06SW30	06SW31	06SW34
<i>Trace elements (ppm)</i>															
Li	6.90	7.99	6.14	8.22	8.23	8.09	8.46	7.13	7.93	9.32	9.91	8.34	7.19	6.15	6.53
Be	2.21	2.12	2.05	2.40	2.21	2.53	2.93	2.50	1.63	2.84	3.09	3.01	1.72	1.60	1.60
Sc	17.5	17.4	18.2	17.6	16.9	16.9	16.9	19.4	19.4	16.1	13.6	14.1	18.6	18.2	20.1
V	181	178	176	183	177	198	217	199	232	202	165	177	169	174	177
Cr	222	221	234	212	211	320	335	276	312	413	402	463	271	267	259
Co	47.5	47.3	42.9	45.0	47.5	47.7	48.6	44.4	50.3	50.3	53.6	54.0	49.7	47.6	46.9
Ni	201	190	196	189	185	252	238	209	202	276	317	321	226	211	169
Cu	60.8	58.7	55.8	62.1	65.7	55.4	57.0	66.0	65.4	53.8	48.2	48.4	56.3	65.5	155.5
Zn	156	153	152	164	160	157	172	137	129	144	149	145	126	125	122
Ga	22.9	22.4	22.2	23.2	21.3	23.6	24.1	22.9	20.3	23.0	22.9	22.6	20.0	19.6	21.7
Rb	29.5	26.4	25.8	29.5	33.0	35.4	36.8	25.1	25.0	27.0	26.0	24.7	21.9	23.3	10.4
Sr	876	856	742	889	804	889	1070	861	669	1002	1087	1151	615	601	623
Zr	237	233	209	241	221	248	277	221	176	233	247	245	156	149	145
Nb	59.8	58.0	47.6	60.5	56.8	68.5	80.0	59.0	38.7	70.7	80.6	79.3	37.0	36.1	32.3
Cs	0.54	0.39	0.49	0.46	0.60	0.53	0.59	0.60	0.48	1.22	0.81	0.79	0.48	0.56	0.79
Ba	593	561	553	623	520	443	459	383	500	542	445	493	364	334	227
Hf	6.08	5.98	5.53	6.29	5.90	6.50	7.21	5.24	3.88	5.43	5.71	5.85	3.91	3.75	3.59
Ta	3.62	3.53	2.92	3.71	3.51	4.66	5.52	3.72	2.11	4.07	4.76	4.88	2.26	2.15	1.96
Tl	0.09	0.08	0.09	0.07	0.10	0.07	0.06	0.06	0.07	0.10	0.08	0.11	0.06	0.06	0.05
Pb	4.73	4.58	4.68	4.95	4.81	4.64	4.66	4.43	3.80	4.06	3.80	3.80	2.98	3.43	1.75
Bi	0.02	0.02	0.02	0.02	0.02	0.02	0.02	0.02	0.01	0.02	0.02	0.02	0.01	0.01	0.01
Th	6.00	5.85	5.01	6.20	5.84	7.37	7.41	4.83	3.83	6.37	7.67	7.66	3.40	3.30	2.99
U	1.47	1.44	1.23	1.47	1.55	1.66	1.93	1.38	1.00	1.60	2.29	2.17	0.65	0.68	0.95
<i>REE (ppm)</i>															
La	46.0	44.9	39.7	47.6	43.8	46.2	54.2	40.3	30.3	50.4	58.1	56.2	27.0	26.3	28.3
Ce	85.8	83.4	72.8	89.0	80.5	82.4	98.5	77.8	60.8	97.1	112	108	53.6	52.0	54.7
Pr	10.7	10.3	9.09	11.0	10.1	10.1	11.9	9.14	7.51	11.3	12.9	12.5	6.54	6.33	6.47
Nd	41.7	39.7	35.6	42.7	39.7	40.9	48.3	36.0	30.8	44.4	49.5	48.4	26.4	25.6	25.7
Sm	9.42	9.06	8.07	9.67	9.07	9.17	9.99	8.10	7.20	9.54	10.42	10.22	6.33	6.10	6.02
Eu	2.76	2.70	2.41	2.86	2.62	2.81	3.16	2.60	1.90	2.78	3.16	2.90	1.93	1.87	1.86
Gd	7.70	7.76	6.84	7.93	7.44	8.04	8.88	7.63	5.96	8.26	8.77	7.96	5.67	5.32	5.44
Tb	1.12	1.08	1.01	1.14	1.08	1.18	1.26	1.08	0.88	1.12	1.17	1.10	0.84	0.78	0.82
Dy	5.97	5.84	5.47	6.11	5.85	5.93	6.13	5.53	4.75	5.31	5.51	5.19	4.37	4.19	4.45
Ho	1.08	1.05	1.01	1.10	1.05	1.07	1.06	0.97	0.87	0.88	0.88	0.86	0.78	0.74	0.80
Er	2.38	2.37	2.30	2.48	2.36	2.53	2.37	2.25	2.15	2.01	2.01	1.92	1.89	1.82	1.97
Tm	0.31	0.31	0.31	0.33	0.31	0.34	0.29	0.28	0.29	0.25	0.24	0.24	0.26	0.25	0.27
Yb	1.83	1.81	1.79	1.82	1.84	2.07	1.61	1.54	1.74	1.37	1.31	1.33	1.50	1.42	1.58
Lu	0.24	0.24	0.24	0.24	0.24	0.29	0.22	0.21	0.25	0.18	0.17	0.17	0.20	0.20	0.22
Y	24.9	24.8	23.8	25.7	24.2	24.1	24.3	23.3	20.6	22.3	22.1	22.4	19.6	19.1	20.3

(continued on next page)

Table 2 (continued)

Lithology sample	Alkali basalt					Tholeiite							Standards		
	06SW35	05WD11	05WD18	05WD22	06SW25	05WD05	05WD36	05WD39	05WD41	06SW26	06SW28	06SW33	GSR-1	GSR-2	GSR-3
<i>Trace elements (ppm)</i>															
Li	8.33	7.07	6.61	6.79	7.41	5.67	4.96	6.33	8.06	5.22	5.93	6.01	131	16.4	9.63
Be	1.84	2.39	1.90	1.76	1.95	1.40	1.51	1.05	1.55	1.65	1.14	1.35	12.5	1.13	2.40
Sc	19.5	17.9	18.2	18.9	16.3	20.0	21.0	19.1	18.5	20.0	20.0	22.1	7.01	7.64	14.8
V	161	186	180	182	146	166	164	168	179	207	157	173	23.4	94.6	162
Cr	359	225	286	290	236	274	299	298	266	269	239	234	4.10	29.7	131
Co	52.8	44.5	49.2	44.2	44.0	45.1	50.1	47.4	43.1	45.4	45.0	40.9	3.30	12.9	44.8
Ni	246	183	215	188	167	211	171	219	218	207	162	134	2.11	15.2	136
Cu	63.6	64.4	62.4	68.0	73.4	71.1	81.2	61.3	69.8	53.7	50.5	65.8	1.04	55.3	50.4
Zn	124	166	152	132	119	127	124	109	129	127	101	99	23.0	53.6	151
Ga	21.6	23.7	21.6	20.4	21.4	21.4	21.3	19.2	20.1	20.3	20.1	19.7	20.1	18.2	24.1
Rb	16.4	20.1	22.0	18.4	15.5	18.2	20.0	13.7	21.0	13.5	12.4	16.8	47.0	37.6	37.7
Sr	644	895	745	620	720	497	523	418	652	619	370	439	107	785	1099
Zr	155	244	204	185	163	168	156	121	165	166	136	141	166	98.7	280
Nb	36.0	60.5	46.6	44.5	36.6	25.4	29.0	19.5	34.6	47.1	22.1	23.9	41.5	5.80	68.2
Cs	0.43	0.53	0.27	0.19	0.42	0.21	0.15	0.22	0.22	1.28	0.21	0.34	38.4	2.09	0.46
Ba	228	639	468	413	254	565	410	301	494	535	217	255	322	1022	542
Hf	3.73	6.26	5.45	4.81	3.94	4.64	4.31	3.35	4.51	4.22	3.40	3.48	6.05	2.83	7.03
Ta	2.15	3.65	3.02	2.79	2.25	1.59	1.83	1.27	2.13	2.87	1.42	1.49	7.09	0.40	4.37
Tl	0.07	0.06	0.06	0.06	0.06	0.08	0.06	0.07	0.05	0.05	0.06	0.06	1.95	0.16	0.06
Pb	2.96	5.66	3.78	3.51	3.06	3.55	3.07	4.83	3.74	3.31	3.02	2.52	31.2	10.8	5.05
Bi	0.02	0.02	0.02	0.02	0.01	0.01	0.01	0.02	0.01	0.02	0.01	0.01	0.52	0.08	0.02
Th	3.28	6.05	4.28	3.84	3.59	3.16	2.78	1.98	3.28	4.29	2.01	2.06	52.0	2.56	6.27
U	1.03	1.49	1.25	0.96	1.00	0.57	0.63	0.34	0.78	1.05	0.26	0.45	18.4	0.89	1.50
<i>REE (ppm)</i>															
La	30.4	46.8	38.4	31.6	36.1	28.1	24.1	17.0	29.4	31.9	16.0	18.4	55.5	22.2	57.0
Ce	58.2	88.6	66.7	57.2	68.2	52.4	44.0	31.4	54.4	61.4	31.2	35.9	109	40.7	107
Pr	6.74	11.0	8.28	7.12	7.81	6.53	5.67	4.09	6.88	7.30	3.80	4.44	13.1	5.02	13.3
Nd	26.7	42.9	33.8	29.0	30.6	25.9	24.0	17.1	28.2	29.4	16.3	18.9	45.5	19.4	53.2
Sm	6.16	9.55	7.97	6.86	7.00	6.27	6.02	4.41	6.67	6.83	4.11	4.57	9.54	3.43	10.5
Eu	1.90	2.83	2.54	2.18	2.19	1.91	1.95	1.47	2.10	2.14	1.43	1.61	0.80	1.09	3.26
Gd	5.68	7.92	7.23	6.21	6.56	5.64	5.65	4.28	5.94	6.16	4.27	4.56	8.61	2.62	8.84
Tb	0.82	1.15	1.07	0.94	0.94	0.85	0.89	0.70	0.89	0.90	0.67	0.72	1.54	0.35	1.21
Dy	4.28	6.08	5.39	4.91	4.89	4.85	4.77	3.86	4.56	4.74	3.95	4.12	9.76	1.78	5.60
Ho	0.77	1.09	0.96	0.90	0.84	0.93	0.90	0.73	0.82	0.85	0.77	0.75	2.12	0.32	0.93
Er	1.88	2.41	2.20	2.16	2.01	2.23	2.18	1.78	1.94	2.04	1.94	1.89	6.16	0.84	2.03
Tm	0.26	0.32	0.29	0.29	0.27	0.31	0.30	0.25	0.26	0.28	0.27	0.28	1.04	0.13	0.25
Yb	1.47	1.79	1.63	1.68	1.53	1.87	1.73	1.52	1.51	1.59	1.62	1.59	7.36	0.85	1.37
Lu	0.21	0.24	0.22	0.23	0.22	0.26	0.25	0.22	0.21	0.22	0.23	0.23	1.11	0.12	0.18
Y	19.7	26.0	22.8	21.5	20.6	23.0	21.7	17.9	19.3	21.8	19.4	19.6	63.6	8.82	21.3

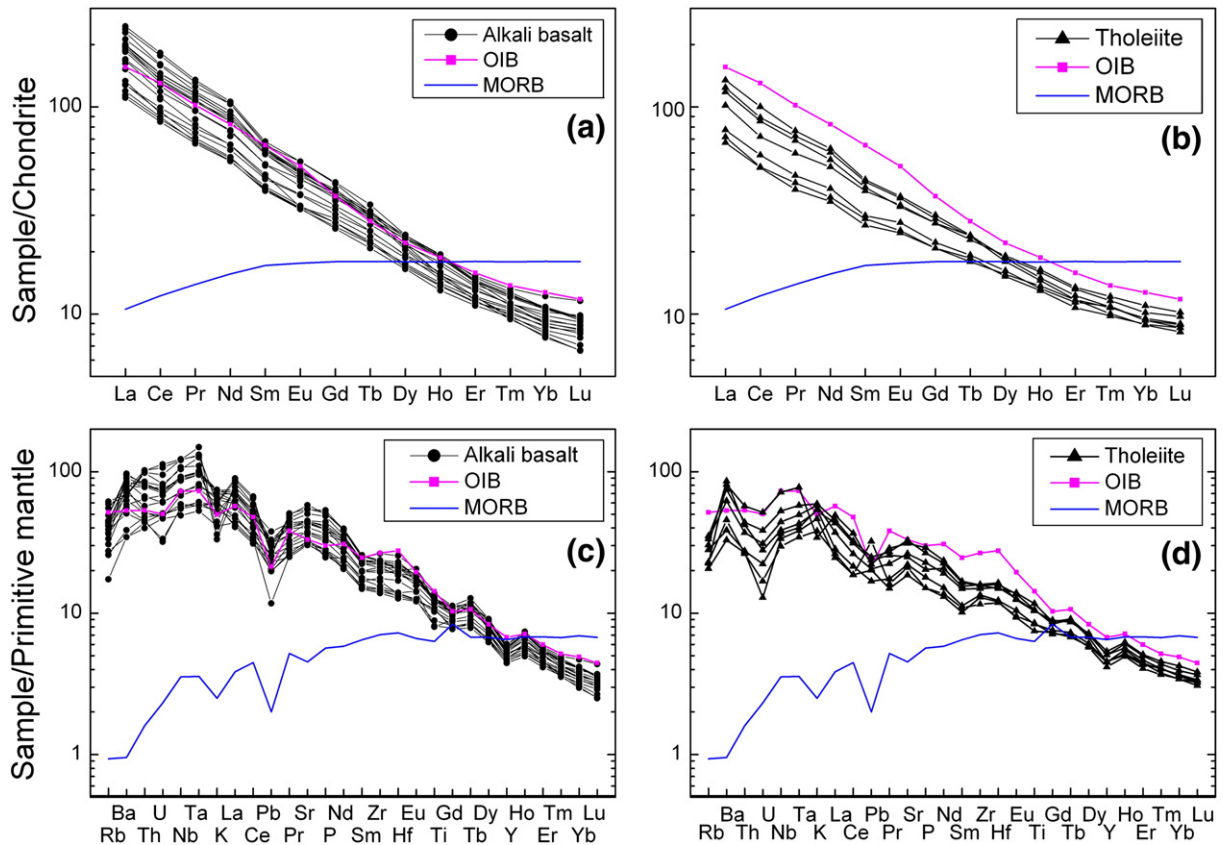


**Fig. 4.** Plots of REE and trace element distribution patterns for Cenozoic basalts in Wan-Su. (a) and (b) Chondrite-normalized REE patterns for alkali basalt and tholeiite, respectively. The chondritic compositions are after Sun and McDonough (1989). (c) and (d) Primitive mantle-normalized trace element patterns for alkali basalt and tholeiite, respectively. The primitive mantle compositions are after McDonough and Sun (1995).

This is particularly so for water-soluble elements such as large ion lithophile elements (LILE) and light rare earth elements (LREE). Petrographically, some olivine phenocrysts exhibit partial alteration to the low-T iddingsite. In addition, the Wan-Su basalts have variable LOI values of 0.03 to 4.91% (Table 1), suggesting variable concentration of volatile elements in the studied samples. The lowest LOI values of 0.03% and 0.77% for samples 06SW35 and 06SW34 correspond to relatively low Pb and U contents (Table 2), indicating no correlation between the LILE variations and the alteration. Furthermore, as illustrated in Fig. 7, the effect of post-magmatic alteration can be minimised by the presence of negative correlations between Th, U, La and SiO<sub>2</sub> because positively correlated trends would be expected for subsolidus alteration.

### 6.1. Crystal fractionation

The Wan-Su basalts contain variable proportions of olivine, clinopyroxene and plagioclase phenocrysts. Ni displays a positive correlation with MgO (Fig. 8a), suggesting fractional crystallization of olivine. This can also be illustrated by a significant correlation between MgO and SiO<sub>2</sub> (Fig. 3c), as well as a correlation between Fe<sub>2</sub>O<sub>3</sub> and SiO<sub>2</sub> (Fig. 3e). Positive correlations also exist between Cr and MgO (Fig. 8b) and between CaO/Al<sub>2</sub>O<sub>3</sub> and MgO (Fig. 8c), suggesting fractional crystallization of clinopyroxene (Green, 1980). However, significant removal of plagioclase did not occur because of the lack of negative Eu anomalies (Fig. 4) and the presence of a positive correlation between Nb and Sr (Fig. 9a). Fractional crystallization of olivine and clinopyroxene can be responsible for the variations in abundances of some major and trace elements such as MgO, Fe<sub>2</sub>O<sub>3</sub>, CaO, Ni and Cr. However, fractional crystallization cannot explain the variations in Sr–Nd–Hf isotopic compositions (Fig. 5). Furthermore, MgO contents

are correlated negatively with initial <sup>87</sup>Sr/<sup>86</sup>Sr ratios but positively with  $\epsilon_{\text{Nd}}(t)$  and  $\epsilon_{\text{Hf}}(t)$  values (Fig. 10), suggesting two-component mixing processes. Therefore, more complex factors or processes are required to assess the petrogenesis of the Wan-Su basalts.

### 6.2. Partial melting

The pressure of peridotite melting has an effect on degree of silica saturation in basaltic magmas (Takahashi and Kushiro, 1983; Langmuir et al., 1992; Kushiro, 2001). Specifically, small degrees of melting (<5% by weight) at high pressures (>3 GPa) produces alkalic magmas with normative nepheline, whereas larger degrees of melting at shallow depths generates tholeiitic magmas with normative hyperthene and quartz (Hirose and Kushiro, 1993; DePaolo and Daley, 2000). CIPW calculations show the presence of the normative hyperthene + quartz in the Wan-Su tholeiite, and the normative nepheline + olivine or normative olivine + hyperthene in the alkali basalt (Table S2). Thus, the tholeiite could form by larger degrees of peridotite melting than the alkali basalt. However, the difference in melting degree cannot explain the differences in Sr–Nd–Hf isotopes between the two types of basalts (Fig. 5). On the other hand, the alkali basalt has lower SiO<sub>2</sub> (40.57 to 48.31 wt.%) but higher MgO (5.41 to 12.10 wt.%) than those of the tholeiite (48.28 to 51.84 wt.% and 3.86 to 6.59 wt.%, respectively) (Table 1). Such differences in lithochemistry can result from near-solidus partial melting of different pyroxenites (Yaxley and Green, 1998; Hirschmann et al., 2003; Kogiso et al., 2003; Pertermann and Hirschmann, 2003; Kogiso and Hirschmann, 2006), with the alkali basalt from silica-deficient pyroxenite and the tholeiite from silica-excess pyroxenite.

Two samples of the alkali basalt (06SW21 and 06SW23) show the highest LREE/HREE ratios with (La/Yb)<sub>N</sub> values of 31.84 and 30.25

**Table 3**  
Whole-rock Rb–Sr isotope compositions of Cenozoic basalts in Wan–Su.

Sample	Rb (ppm)	Sr (ppm)	<sup>87</sup> Rb/ <sup>86</sup> Sr	<sup>87</sup> Sr/ <sup>86</sup> Sr	Error (2σ)	<i>t</i> <sub>Sr</sub> (t = 16 Ma)
<i>Alkali basalt</i>						
05WD06	29.71	911.8	0.0942	0.704104	0.000011	0.704083
05WD08	26.35	886.2	0.0860	0.704095	0.000012	0.704076
05WD09	26.02	775.7	0.0970	0.704270	0.000014	0.704248
05WD15	29.46	930.4	0.0916	0.704009	0.000011	0.703988
05WD16	32.90	831.3	0.1145	0.703931	0.000014	0.703905
05WD31	35.33	941.2	0.1086	0.703582	0.000012	0.703558
05WD33	36.71	1137	0.0933	0.703666	0.000014	0.703645
06WD38	25.09	946.8	0.0766	0.704123	0.000013	0.704106
05WD42	24.25	664.0	0.1056	0.704482	0.000013	0.704458
06SW19	25.59	1078	0.0686	0.703494	0.000012	0.703478
06SW21	25.67	1216	0.0611	0.703284	0.000011	0.703271
06SW23	24.40	1244	0.0567	0.703453	0.000012	0.703440
06SW30	22.91	660.6	0.1003	0.704089	0.000011	0.704066
06SW31	23.91	672.2	0.1029	0.704071	0.000012	0.704048
06SW34	11.95	677.9	0.0510	0.703633	0.000015	0.703622
06SW35	17.34	689.5	0.0727	0.703596	0.000012	0.703580
05WD11	20.17	940.6	0.0620	0.704132	0.000013	0.704118
05WD18	22.18	784.4	0.0818	0.703937	0.000014	0.703919
05WD22	18.51	665.0	0.0805	0.704316	0.000013	0.704298
06SW25	15.96	781.9	0.0590	0.703768	0.000013	0.703755
<i>Tholeiite</i>						
05WD05	18.43	524.9	0.1015	0.705018	0.000013	0.704995
05WD36	20.25	553.8	0.1058	0.704993	0.000013	0.704969
05WD39	14.01	447.5	0.0906	0.704899	0.000012	0.704879
05WD41	21.69	702.1	0.0894	0.704498	0.000012	0.704478
06SW26	15.10	683.6	0.0639	0.704246	0.000013	0.704231
06SW28	13.96	404.0	0.1000	0.704725	0.000011	0.704702
06SW33	15.90	481.9	0.0954	0.704400	0.000010	0.704378

(Table S3), respectively. This indicates that they were derived from low-degree melts. It is known that clinopyroxene and garnet begin to melt before olivine and orthopyroxene during mantle melting

**Table 4**  
Whole-rock Sm–Nd isotope compositions of Cenozoic basalts in Wan–Su.

Sample	Sm (ppm)	Nd (ppm)	<sup>147</sup> Sm/ <sup>144</sup> Nd	<sup>143</sup> Nd/ <sup>144</sup> Nd	Error (2σ)	<i>t</i> = 16 Ma	<i>T</i> <sub>DM1</sub>	
						<sup>143</sup> Nd/ <sup>144</sup> Nd <sub>t</sub>	<i>ε</i> <sub>Nd</sub> ( <i>t</i> )	
<i>Alkali basalt</i>								
05WD06	8.610	38.48	0.1353	0.512667	0.000010	0.512653	0.70	941
05WD08	8.501	37.83	0.1359	0.512679	0.000011	0.512665	0.94	924
05WD09	7.610	33.49	0.1374	0.512554	0.000011	0.512540	−1.51	1191
05WD15	8.894	40.00	0.1344	0.512671	0.000009	0.512657	0.78	923
05WD16	8.139	35.84	0.1373	0.512723	0.000009	0.512708	1.78	854
05WD31	8.473	38.50	0.1330	0.512887	0.000012	0.512873	5.00	499
05WD33	9.846	46.19	0.1289	0.512900	0.000012	0.512887	5.27	451
06WD38	8.039	36.06	0.1348	0.512842	0.000010	0.512828	4.12	597
05WD42	5.929	25.82	0.1388	0.512531	0.000011	0.512517	−1.96	1260
06SW19	9.016	42.39	0.1286	0.512940	0.000010	0.512927	6.05	378
06SW21	10.36	49.66	0.1261	0.512983	0.000011	0.512970	6.89	293
06SW23	9.412	45.02	0.1264	0.512966	0.000010	0.512952	6.54	324
06SW30	5.927	25.22	0.1421	0.512751	0.000012	0.512737	2.33	851
06SW31	6.116	26.04	0.1420	0.512749	0.000012	0.512734	2.29	854
06SW34	5.779	24.98	0.1398	0.512899	0.000011	0.512884	5.21	521
06SW35	5.912	25.98	0.1376	0.512897	0.000011	0.512883	5.18	509
05WD11	9.040	40.54	0.1348	0.512657	0.000009	0.512643	0.51	954
05WD18	7.611	32.66	0.1409	0.512823	0.000012	0.512808	3.72	688
05WD22	6.591	28.56	0.1395	0.512648	0.000012	0.512633	0.31	1034
06SW25	6.702	30.20	0.1342	0.512915	0.000011	0.512901	5.54	453
<i>Tholeiite</i>								
05WD05	5.832	24.70	0.1427	0.512239	0.000012	0.512224	−7.67	1953
05WD36	5.504	22.64	0.1470	0.512475	0.000012	0.512460	−3.07	1540
05WD39	4.145	16.44	0.1524	0.512421	0.000015	0.512405	−4.14	1811
05WD41	6.208	27.00	0.1390	0.512525	0.000012	0.512510	−2.08	1276
06SW26	6.655	29.08	0.1383	0.512744	0.000011	0.512729	2.19	824
06SW28	4.004	15.69	0.1543	0.512558	0.000010	0.512542	−1.47	1519
06SW33	4.458	18.12	0.1488	0.512615	0.000011	0.512599	−0.35	1258

**Table 5**  
Whole-rock Lu–Hf isotope compositions of Cenozoic basalts in Wan–Su.

Sample	Lu (ppm)	Hf (ppm)	<sup>176</sup> Lu/ <sup>177</sup> Hf	<sup>176</sup> Hf/ <sup>177</sup> Hf	Error (2σ)	<i>t</i> = 16 Ma	<i>T</i> <sub>DM1</sub>	
						<sup>176</sup> Hf/ <sup>177</sup> Hf <sub>t</sub>	<i>ε</i> <sub>Hf</sub> ( <i>t</i> )	
<i>Alkali basalt</i>								
05WD06	0.242	6.076	0.00566	0.282865	0.000010	0.282863	3.58	627
05WD08	0.238	5.978	0.00565	0.282888	0.000012	0.282886	4.40	589
05WD09	0.243	5.529	0.00624	0.282804	0.000009	0.282802	1.42	739
05WD15	0.237	6.289	0.00535	0.282855	0.000006	0.282853	3.23	637
05WD16	0.244	5.895	0.00588	0.282870	0.000007	0.282868	3.76	623
05WD31	0.294	6.498	0.00642	0.282931	0.000009	0.282929	5.91	532
05WD33	0.222	7.207	0.00437	0.282851	0.000009	0.282850	3.10	625
06WD38	0.213	5.244	0.00577	0.282942	0.000006	0.282941	6.32	503
05WD42	0.250	3.877	0.00916	0.282692	0.000007	0.282689	−2.57	1013
06SW19	0.180	5.428	0.00471	0.283017	0.000005	0.283015	8.96	370
06SW21	0.170	5.711	0.00423	0.283080	0.000007	0.283078	11.19	267
06SW23	0.169	5.854	0.00410	0.283061	0.000006	0.283060	10.55	294
06SW30	0.204	3.905	0.00742	0.282863	0.000007	0.282861	3.50	665
06SW31	0.195	3.750	0.00738	0.282868	0.000009	0.282866	3.67	656
06SW34	0.224	3.590	0.00886	0.282970	0.000007	0.282968	7.27	505
06SW35	0.209	3.725	0.00797	0.282977	0.000006	0.282975	7.52	479
05WD11	0.243	6.257	0.00551	0.282864	0.000008	0.282862	3.53	626
05WD18	0.222	5.452	0.00578	0.282929	0.000011	0.282927	5.84	525
05WD22	0.232	4.809	0.00685	0.282784	0.000008	0.282782	0.71	786
06SW25	0.215	3.939	0.00775	0.282966	0.000008	0.282964	7.14	494
<i>Tholeiite</i>								
05WD05	0.259	4.638	0.00793	0.282734	0.000024	0.282732	−1.07	900
05WD36	0.247	4.313	0.00813	0.282597	0.000010	0.282595	−5.92	1144
05WD39	0.218	3.351	0.00924	0.282614	0.000013	0.282611	−5.33	1157
05WD41	0.208	4.513	0.00654	0.282616	0.000009	0.282614	−5.23	1057
06SW26	0.219	4.215	0.00738	0.282825	0.000007	0.282823	2.15	730
06SW28	0.228	3.397	0.00953	0.282794	0.000009	0.282791	1.04	840
06SW33	0.226	3.480	0.00922	0.282817	0.000008	0.282815	1.86	789

(Kinzler, 1997). Thus basaltic melts produced from low degrees of peridotite melting are characterized by relatively high SiO<sub>2</sub> and low MgO contents. This generalization is in conflict with the high MgO (12.10% and 12.00%) and low SiO<sub>2</sub> contents (40.57% and 41.04%) for the two samples. It could be resolved by suggesting that their mantle source had previously experienced melt extraction, resulting in harzburgite (e.g., Wagner and Grove, 1998). Low-degree melts of harzburgite-dominated mantle would be capable of having high MgO but low SiO<sub>2</sub> contents. On the other hand, the high (La/Yb)<sub>N</sub> ratios require garnet, a HREE-rich mineral, to be present as a residual phase in the mantle source during partial melting.

In a suite of terrestrial basalts with limited variability in isotopic ratios and significant elemental variation, the effects of variable extents of partial melting can be inferred by plotting abundance ratios involving incompatible elements against the concentration of a highly incompatible element. A constant abundance ratio over a wide range of incompatible element concentration indicates the source ratio (Hofmann et al., 1984), whereas a systematic increase or decrease in abundance ratio reflects the effect of the melting process, specifically the residual minerals that control the bulk-solid/melt partition coefficients (Yang et al., 2003). Because Tb is more incompatible than Yb in garnet (van Westrenen et al., 2000) and the high compatibility of Sr relative to Ce is a characteristic of phlogopite (LaTourrette et al., 1995; Dalpé and Baker, 2000), Yang et al. (2003) suggest that a positive Tb/Yb–Th correlation in basalts reflects the control of residual garnet whereas a negative Sr/Ce–Th correlation reflects the role of phlogopite during mantle melting. Likewise, Sr is much less compatible than Nb in rutile (Foley et al., 2000; Rudnick et al., 2000), so that a negative Sr/Nb–Th correlation reflects the dissolution of rutile. As illustrated in Fig. 11a, the garnet as the residual phase during mantle melting is consistent with the positive Tb/Yb–Th correlation in the Wan–Su basalts. On the other hand, there are inverse Sr/Nb and Sr/Ce versus Th trends for the basalts (Fig. 11b and c), suggesting that rutile

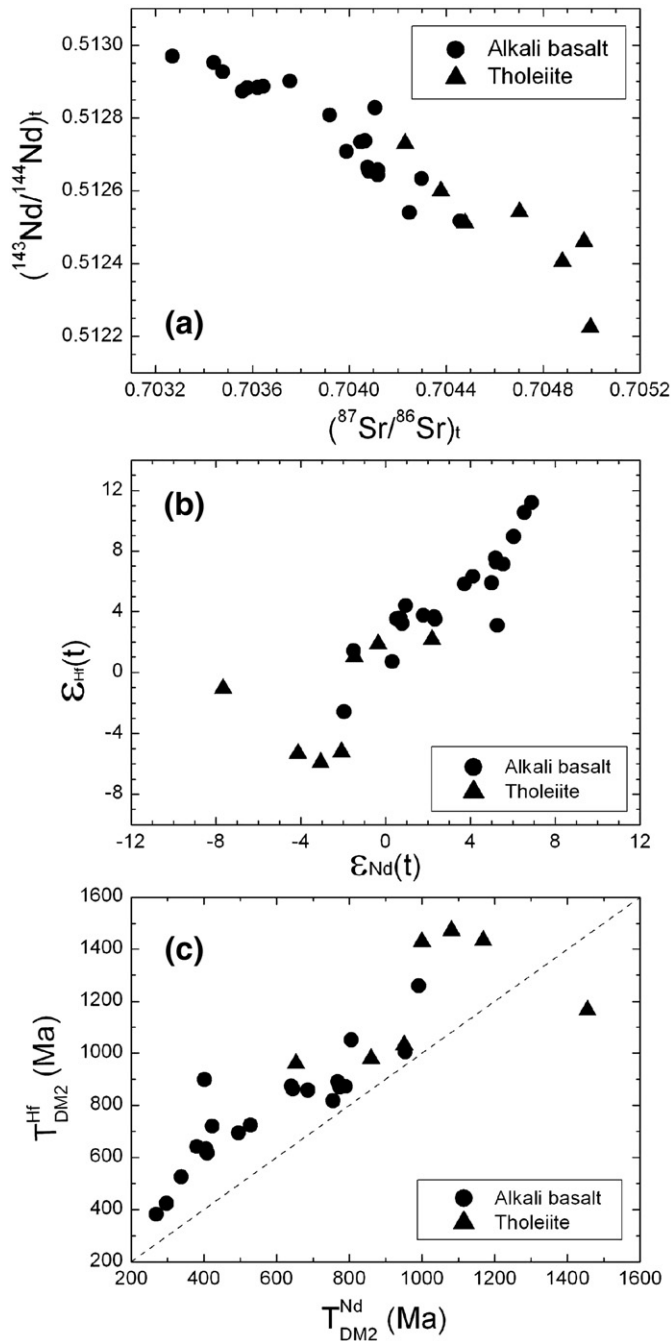


**Fig. 5.** Plots of whole-rock Sr–Hf–Nd isotope relationships for Cenozoic basalts in Wan–Su. (a) Initial Sr and Nd isotopic ratios at  $t = 16$  Ma, (b) initial Nd and Hf isotopic ratios at  $t = 16$  Ma, and (c) single-stage Hf and Nd model ages.

and phlogopite were dissolved during the partial melting. The Wan–Su basalts have subchondritic Nb/Ta ratios of 14.49 to 17.37 (Table S3), consistent with dissolution of rutile during partial melting of eclogite under the conditions of  $> 1250$  °C and 2.0–3.0 GPa (Klemme et al., 2002; Xiong et al., 2005; Liu et al., 2008).

There are positive correlations between Nb and MgO (Fig. 8e) and between Ta and MgO (Fig. 8f) for the Wan–Su basalts, suggesting that both Nb and Ta are compatible during mantle melting and thus significant control of Ti–Fe oxides such as rutile and ilmenite (Liu et al., 2008). Furthermore, there are constant Nb/Ta ratios with respect to the variation in MgO for the basalts (Fig. 8f), reinforcing the role of the Nb- and Ta-rich Ti–Fe oxides during partial melting. However, different degrees of partial melting do not cause variations in

radiogenic isotopic compositions, so that the source nature exerts a fundamental control on the initial Sr, Nd and Hf isotope ratios (Tables 3–5). In particular, the correlations between  $I_{Sr}$ ,  $\epsilon_{Nd}(t)$ ,  $\epsilon_{Hf}(t)$  and MgO (Fig. 10) for the basalts cannot be explained by different degrees of partial melting alone, but may be related to a certain type of mixing processes. While the composition of major elements in the basalts requires the principal contribution from partial melting of peridotite or pyroxenite mantle, the varying  $\epsilon_{Nd}(t)$  and  $\epsilon_{Hf}(t)$  values (Fig. 5a and b) as well as the differing Nd and Hf model ages (Fig. 5c) suggest variable contributions from juvenile depleted to ancient enriched mantle components.

The alkali basalt is significantly more depleted in radiogenic Sr, Nd and Hf isotopes than the tholeiite (Fig. 5a and b). Thus, the alkali basalt was derived from relatively depleted mantle component whereas the tholeiite was originated from relatively enriched mantle component. Furthermore, there is the negative correlation between the initial Sr–Nd isotope ratios (Fig. 5a) and the positive correlation between the initial Nd–Hf isotope ratios (Fig. 5b), suggesting variable degrees of mixing between the two contrasting SCLM sources. It is possible that the alkali basalt could be derived from a young SCLM by the small degrees of peridotite melting, whereas the tholeiite could be derived from an old SCLM by the large degrees of peridotite melting. If the craton SCLM is assumed to be responsible for the old SCLM, high MgO contents should be expected for partial melts of the craton SCLM because of its refractory nature (Wagner and Grove, 1998; Rudnick et al., 2004; Pearson and Wittig, 2008). However, this is in conflict to the observation that the tholeiite has lower MgO contents than the alkali basalt (Table 1). Alternatively, the alkalic and tholeiitic basalts can be derived from the same age of SCLM, with the former from the near-solidus melting of silica-deficient pyroxenite whereas the latter from the near-solidus melting of silica-excess pyroxenite. In either case, there are variable degrees of mixing between the isotopically depleted and enriched components in the SCLM source.

**Table 6**

Oxygen isotope compositions of phenocrysts from Cenozoic basalts in Wan–Su.

Sample	$\delta^{18}O$ (‰)	
	OI	Cpx
<i>Alkali basalt</i>		
05WD08	5.41	5.08
05WD09		5.12
05WD15		4.66
05WD16	4.00	4.80
05WD31	5.76	
06WD38		5.50
05WD42	5.42	4.86
06SW19	5.91	
06SW21	5.35	5.48
06SW23	5.55	4.42
05WD11		5.24
05WD22		5.19
06SW25	4.48	5.50
<i>Tholeiite</i>		
05WD05	5.51	
05WD36		5.70
05WD39		5.62
05WD41		5.13
06SW26		5.32
06SW33		5.02
<i>Basalt (subtype is uncertain)</i>		
05WD04	5.06	
05WD07	5.10	
05WD10	5.20	
05WD12		5.26
05WD14		5.46
05WD17	5.14	
05WD19	5.20	5.04
05WD27	5.61	5.62

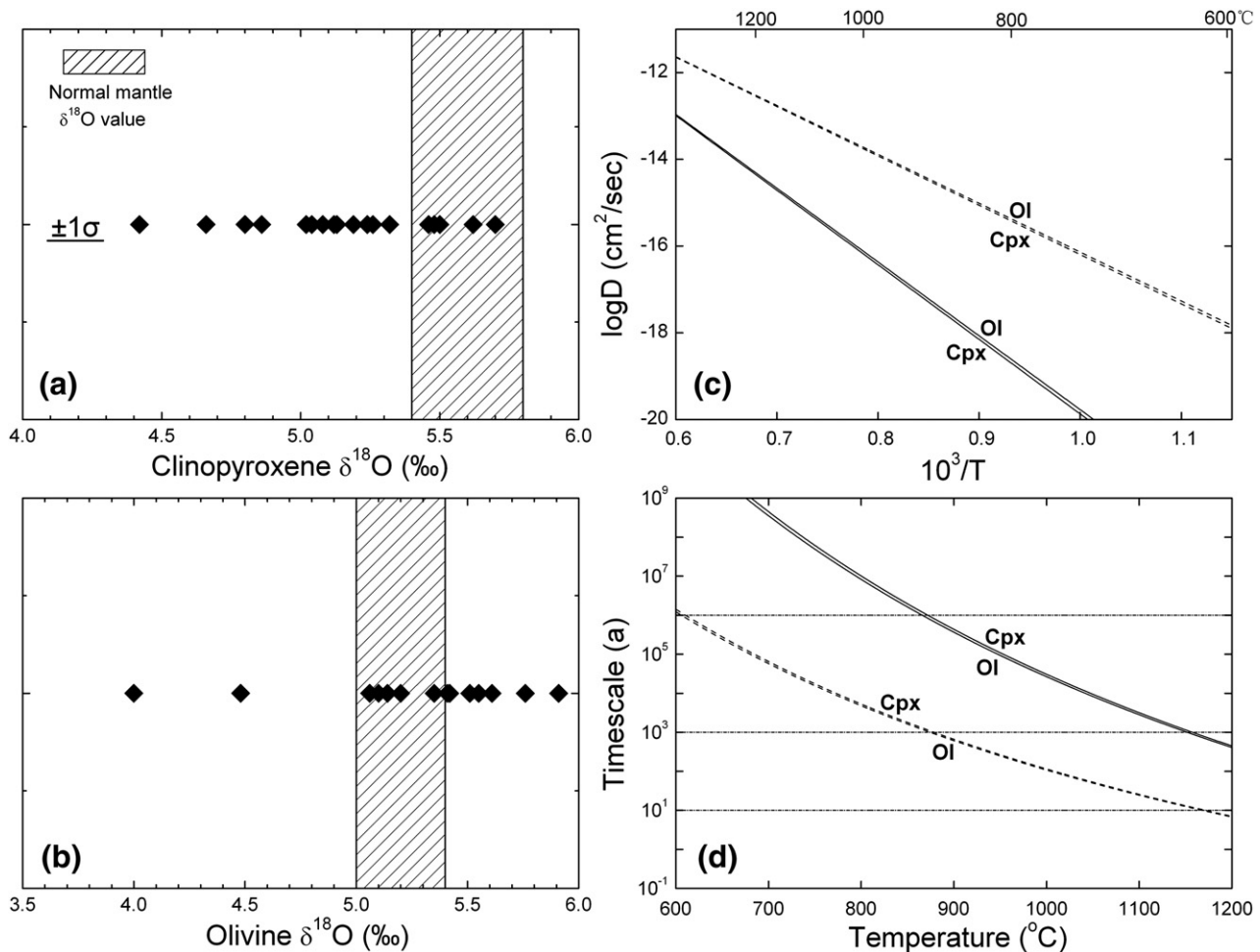


**Fig. 6.** The oxygen isotope composition of phenocrysts from Cenozoic basalts in Wan-Su and its kinetic interpretation via estimation of duration of O isotope homogenization between phenocryst and melt in the mantle. (a) and (b) Phenocryst  $\delta^{18}\text{O}$  values for clinopyroxene and olivine, respectively. (c) Arrhenius plot of empirically predicted oxygen diffusivity in clinopyroxene and olivine under hydrothermal and anhydrous conditions. (d) Timescale of oxygen isotope resetting in clinopyroxene and olivine at different temperatures under hydrothermal or anhydrous conditions with grain radii of 200  $\mu\text{m}$ . Diffusion data are from Zheng and Fu (1998).

### 6.3. Mixing of distinct components

The Wan-Su basalts show the correlations between major elements, trace elements and radiogenic isotopes (Fig. 10). In addition,  $\varepsilon_{\text{Nd}}(t)$  also correlates negatively with Sm/Nd, and  $I_{\text{Sr}}(t)$  correlates positively with 1/Sr (not shown). These correlations reflect mixing of at least two distinct components, which could be achieved by either the contamination of continental crust during magma ascent or the source mixing between distinct mantle components prior to partial melting. In particular, the geochemical signatures of both the subcontinental lithospheric mantle and the subducted oceanic crust are identified in this study.

The Wan-Su basalts show a positive correlation between Nd and Hf model ages (Fig. 5c). The Nd model ages for the alkalic basalts are about 30 to 700 Ma older than the Hf model ages (Tables 4 and 5), with the larger differences occurring in the tholeiites. This may be caused by the effect of differential Sm/Nd and Lu/Hf fractionation or component mixing during melt-peridotite reaction. As a result, the absolute values for Nd or Hf model ages are unlikely to be comparable with radiometric ages in geochronology. Nevertheless, they can be a proxy for relative times of magma extraction from juvenile or ancient mantle source. In particular, the youngest Nd and Hf model ages can be used to approximate the maximum age of melt extraction from the asthenosphere because partial melting of mantle peridotites would decrease Sm/Nd and Lu/Hf ratios of basaltic melts and thus enhance their Nd and Hf model ages. On the other hand, the

oldest Nd and Hf model ages may provide the minimum estimate for the residence time of old mantle components since their separation from the asthenosphere because melt extraction would increase Sm/Nd and Lu/Hf ratios of SCLM and thus reduce its Nd and Hf model ages.

#### 6.3.1. Crustal contamination

Three tholeiite samples (05SW36, 05SW39 and 05SW41) have the most negative  $\varepsilon_{\text{Hf}}(t)$  values of  $-5.23$  to  $-5.92$  (Table 5), which could suggest the maximum involvement of crustal component. However, their  $(\text{La}/\text{Yb})_{\text{N}}$  ratios of 8.03 to 14.0 (Table S3) are lower than those positive  $\varepsilon_{\text{Hf}}(t)$  samples, inconsistent with the incorporation of continental crust, as are their negative Pb anomalies (Fig. 4d). On the other hand, incompatible elements (e.g., Th, La and U) are negatively correlated with  $\text{SiO}_2$  for all the Wan-Su basalts (Fig. 7), implying insignificant interaction with felsic continental crust. In addition, the negative correlation between  $\varepsilon_{\text{Nd}}(t)$  and Sm/Nd is the opposite to that expected from the contamination of continental crust during magma ascent through it. In either case, the crustal contamination is insignificant for the alkali basalts. It is also important to note that the alkalic and tholeiitic basalts have Nb/U ratios of 34.2 to 57.2 and 44.5 to 84.7, respectively (Table S3), significantly higher than the average Nb/U ratios of  $9 \pm 3$  for the continental crust. Therefore, the crustal contamination can be ruled out as a possible mechanism for the observed variations in radiogenic isotopes and correlations between elements and isotopes.

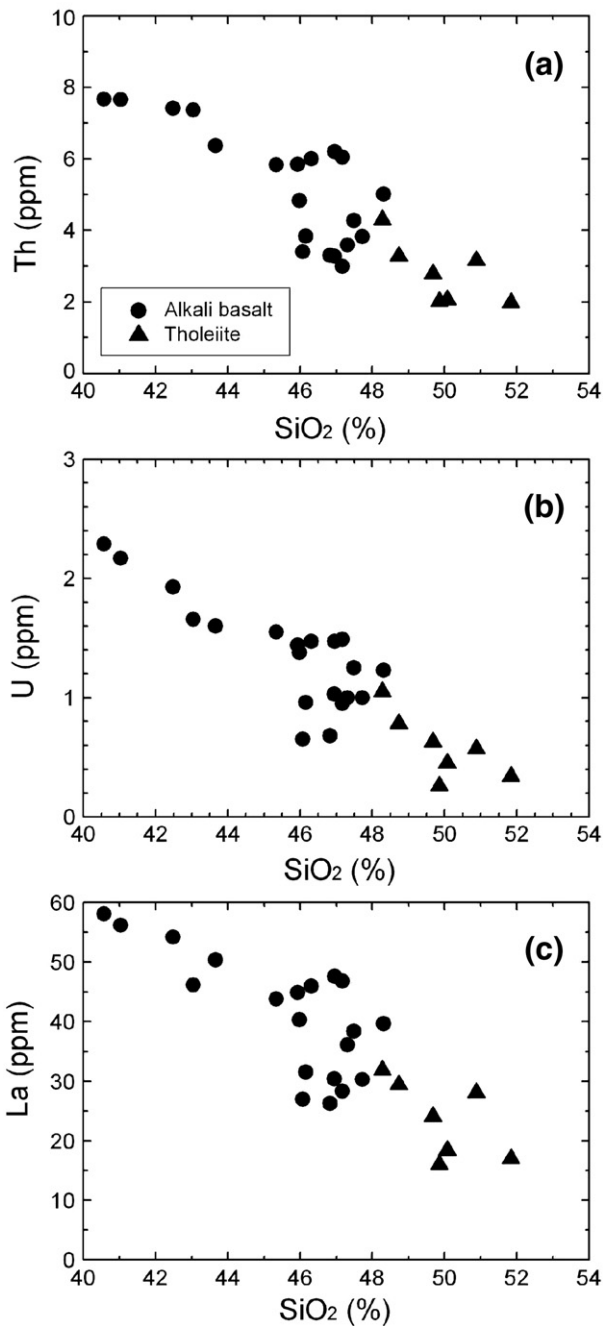


Fig. 7. The relationships between SiO<sub>2</sub> and Th, U or La for Cenozoic basalts in Wan-Su.

### 6.3.2. The nature of magma source

The alkalic and tholeiitic basalts have Mg numbers of 44.9 to 63.5 and 37.1 to 52.5, respectively (Table S3 and Fig. 9b), significantly lower than  $88.2 \pm 0.3$  for Hawaiian OIB and  $89.8 \pm 0.2$  for MORB (Humayun et al., 2004). They show Fe/Mn ratios of 69.54 to 87.68 and 71.11 to 78.15 (Table S3 and Fig. 9b), respectively, which are higher than  $66.9 \pm 1.8$  for Hawaiian OIB and  $56.5 \pm 1.1$  for MORB (Humayun et al., 2004). Because most of the Fe in the mantle is Fe<sup>2+</sup> (FeO) and all of the Mn is Mn<sup>2+</sup> (MnO), Fe and Mn share the same charge and ionic radius, and have similar partitioning behaviour in magmatic processes (Humayun et al., 2004). Experimental studies of partial melting of pyroxenite and peridotite show that the Fe/Mn ratios for pyroxenite melts are higher than those for peridotite melts because clinopyroxene, orthopyroxene and garnet all have  $D(\text{Fe}) > D(\text{Mn})$  whereas olivine has  $D(\text{Fe}) < D(\text{Mn})$  (Walter, 1998; Pertermann and

Hirschmann, 2003). It is also known that partial melting of pyroxenite can produce alkalic to tholeiitic transition in ocean island basalts (Hirschmann et al., 2003; Keshav et al., 2004). Thus it is possible that the high Fe/Mn ratios for the Wan-Su basalts (Fig. 9b) result from partial melting of pyroxenites in the mantle source (Herzberg, 2006; Sobolev et al., 2007). This is also consistent with the low Mg numbers (Fig. 9b) and the low CaO contents (Table 1) for these basalts, suggesting predominant contribution of pyroxenites to the continental basalts.

The Wan-Su basalts have very similar chondrite-normalized REE patterns and primitive mantle-normalized trace element patterns to OIB, but remarkably distinctive from MORB (Fig. 4). They show LREE enrichment but HREE depletion, no depletion in Nb and Ta but negative Pb anomalies on a primitive mantle-normalized plot. They have the high Fe/Mn ratios and the subchondritic Nb/Ta ratios. The alkalic and tholeiitic basalts have (La/Yb)<sub>N</sub> ratios of 12.5 to 31.8 and 7.07 to 14.4 (Table S3), respectively; their Nb/U ratios mostly within the field of OIB (Nb/U =  $47 \pm 10$ ), except tholeiite 06SW28 with the anomalously high Nb/U ratio of 84.7 (likely due to U loss). A Nb/Y vs Zr/Y plot has been used to distinguish OIB from MORB lavas in Iceland and other areas (Fitton et al., 1997; Fitton, 2007). It can be also used to test whether the Wan-Su basalts were derived from the MORB-type mantle source (Fig. 9c). Fitton et al. (1997) defined  $\Delta\text{Nb} = 1.74 + \log(\text{Nb}/\text{Y}) - 1.92 \log(\text{Zr}/\text{Y})$  as a geochemical parameter to characterise the mantle source and to minimize the effects of melting degrees, source depletion through melt extraction, or supracrustal processes (e.g., subsolidus alteration). Fitton (2007) found that virtually all Icelandic basalts have  $\Delta\text{Nb} > 0$  whereas all N-MORB has  $\Delta\text{Nb} < 0$ . The calculated  $\Delta\text{Nb}$  values for the Wan-Su alkalic and tholeiitic basalts are 0.22 to 0.30 and 0.13 to 0.38, respectively (Table 2), suggesting that they cannot be derived from partial melting of the asthenosphere, the typical mantle source of MORB.

Clinopyroxene phenocrysts from the Wan-Su basalts possess  $\delta^{18}\text{O}$  values of 4.4‰ to 5.7‰ (Fig. 6a), most of which are lower than the normal upper mantle values of  $5.6 \pm 0.2\text{‰}$ . Olivine phenocrysts from two samples 05WD16 and 06SW25 have  $\delta^{18}\text{O}$  values of 4.0‰ and 4.5‰ (Fig. 6b), respectively, significantly lower than the normal mantle values of  $5.2 \pm 0.2\text{‰}$ . This suggests that the alkali basalt acquired the low  $\delta^{18}\text{O}$  signature from the magma source because mineral  $\delta^{18}\text{O}$  values lower than the normal upper mantle values must result from water-rock interaction at high temperatures (e.g., Gautason and Muehlenbachs, 1998; Zheng et al., 1998; Wang et al., 2003). The equilibrium O isotope fractionations between minerals are small at mantle temperatures (Chiba et al., 1989; Zheng, 1993), so that the low  $\delta^{18}\text{O}$  phenocrysts were crystallized from low  $\delta^{18}\text{O}$  magmas. Thus, the basalt source appears to be depleted in <sup>18</sup>O before extensive melting (Eiler, 2001). The source <sup>18</sup>O depletion can be caused by either recycling of Neoproterozoic low  $\delta^{18}\text{O}$  igneous rocks in the South China Block, or partial melting of the dehydrated oceanic crust that experienced high-T seawater-rock interaction during its original emplacement as MORB.

According to the study of Rumble et al. (2002), Zheng et al. (2004, 2007) and Tang et al. (2008a,b), zircons show variable  $\delta^{18}\text{O}$  values of  $-10.9\text{‰}$  to  $8.5\text{‰}$  from granitoid, granitic gneiss and eclogite in the Dabie-Sulu orogenic belt, east-central China. Most of the  $\delta^{18}\text{O}$  values are lower than normal mantle zircon values of  $5.3 \pm 0.3\text{‰}$  (Valley et al., 1998). The low  $\delta^{18}\text{O}$  zircons mostly have protolith ages of 740 to 780 Ma, corresponding to the time of rifting the South China Block from the supercontinent Rodinia (Li et al., 2003; Zheng et al., 2006). One might expect if phenocrysts with low  $\delta^{18}\text{O}$  values for the Wan-Su basalts could be correlated with the Neoproterozoic low  $\delta^{18}\text{O}$  igneous rocks, the shallow mantle in east-central China would be overprinted by the low  $\delta^{18}\text{O}$  fluid released from the Neoproterozoic low  $\delta^{18}\text{O}$  rocks during the Triassic subduction of the South China Block beneath the North China Block. Compared to the Cenozoic basalts from Wan-Su, however, Neoproterozoic igneous rocks in the Dabie-Sulu orogenic

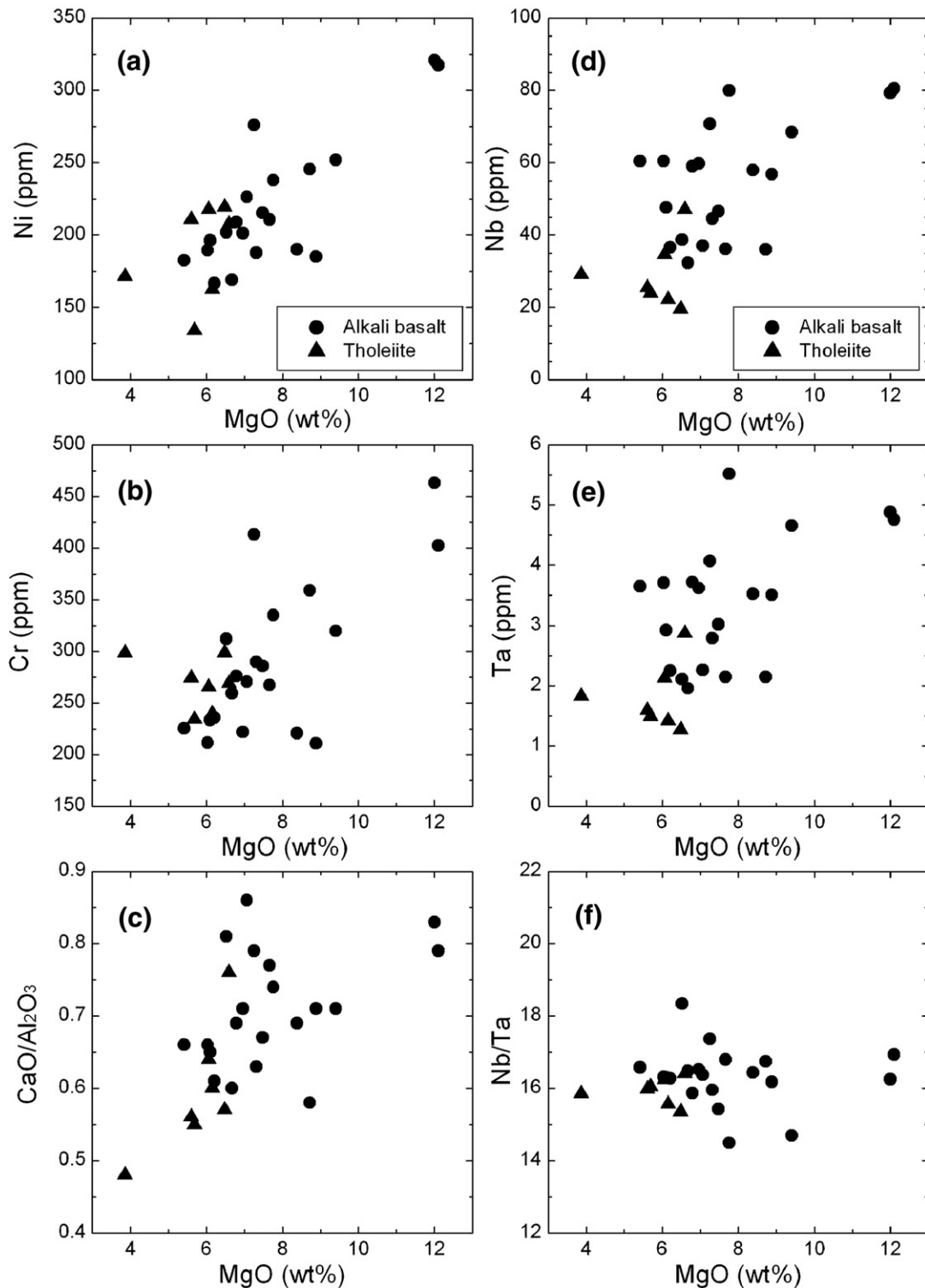


**Fig. 8.** Plots of MgO versus element concentrations and ratios for Cenozoic basalts in Wan-Su. (a), (b) and (c) Correlative variations between Ni, Cr, CaO/Al<sub>2</sub>O<sub>3</sub> and MgO for fractional crystallization of olivine and clinopyroxene. (d), (e) and (f) Correlative variations between Nb, Ta, Nb/Ta and MgO for the role of Ti-Fe oxides during mantle melting.

belt are principally of felsic composition (Zheng, 2008) and have much higher initial Sr isotopic ratios but lower initial Nd isotopic ratios (Jahn, 1998; Chen et al., 2002a; Huang et al., 2006; Tang et al., 2008a). On the other hand, the basalts, especially the alkalic ones, have the positive  $\epsilon_{Nd}(t)$  and  $\epsilon_{Hf}(t)$  values (Fig. 5b) and thus the very young Nd and Hf model ages (Tables 4 and 5). For example, sample 06SW23 has a clinopyroxene  $\delta^{18}O$  value of 4.42‰, with a young Nd model age of 324 Ma and a Hf model age of 294 Ma. These obser-

vations could be explained by the contribution from the Late Paleozoic to Early Mesozoic SCLM that was overprinted by the low  $\delta^{18}O$  aqueous fluid or hydrous melt. However, the involvement of aqueous fluid would lead to the trace element characteristics of oceanic arc basalts (Hawkesworth et al., 1991; Tatsumi and Eggins, 1995), and the involvement of felsic melt would result in an increase in SiO<sub>2</sub>, and older Nd and Hf model ages for the alkali basalts. Therefore, the former is not consistent with their OIB-like trace element characteristics,

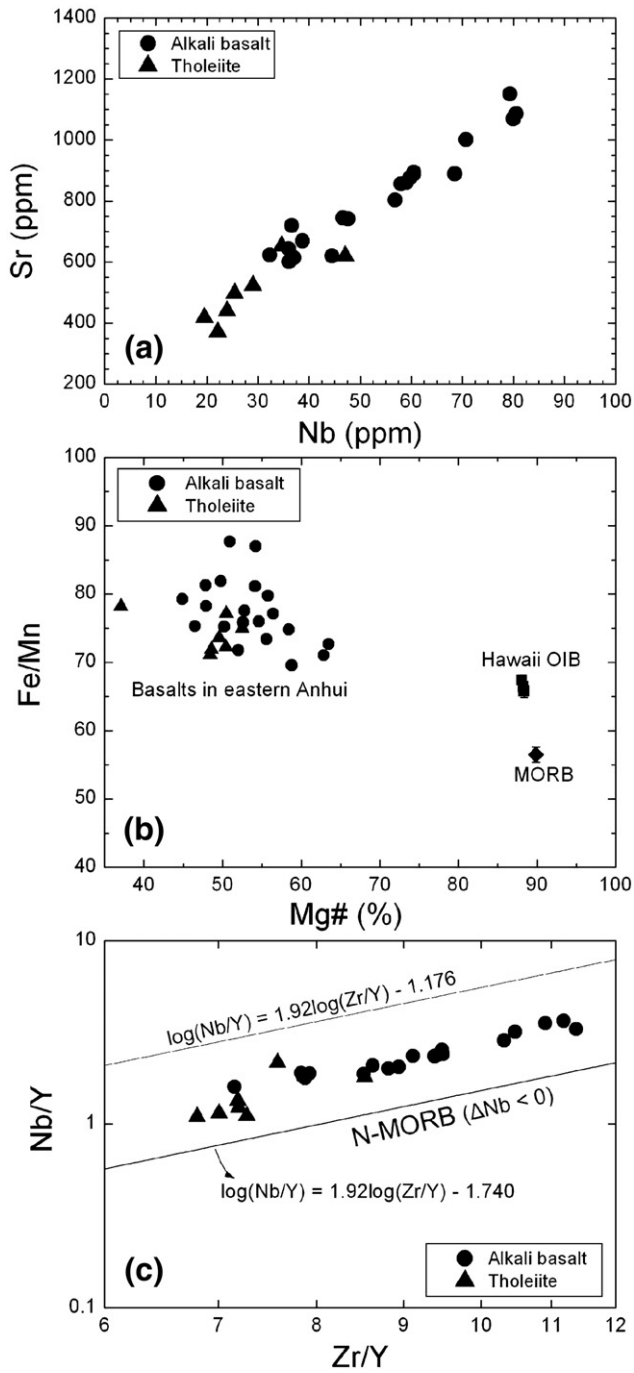


**Fig. 9.** Plots of Nb versus Sr abundances (a), Mg number versus Fe/Mn ratio (b), and Nb/Y versus Zr/Y (c) for Cenozoic basalts in Wan–Su. Hawaiian OIB has Mg numbers of  $88.2 \pm 0.3$  and Fe/Mn ratios of  $66.9 \pm 1.8$ , and MORB has Mg numbers of  $89.8 \pm 0.2$  and Fe/Mn ratios of  $56.5 \pm 1.1$  (Humayun et al., 2004); the error ( $\sigma$ ) is denoted as the bar. The  $\Delta Nb$  calculations follow the definition of Fitton et al. (1997), with  $\Delta Nb < 0$  for N-MORB.

whereas the latter is not favoured by their silica deficiency and depletion of Nd–Hf isotopes. These conflicts could be reconciled by hypothesizing involvement of the low  $\delta^{18}\text{O}$  mafic melt instead of the low  $\delta^{18}\text{O}$  aqueous fluid or felsic melt, but no petrological and geochemical observations support this hypothesis at present.

Alternatively, the phenocryst oxygen isotope compositions can be produced by melting of the subducted oceanic crust that underwent isotopic exchange with seawater during MORB-type magma emplacement at high temperatures (e.g., Gautason and Muehlenbachs, 1998; Eiler, 2001; Wang et al., 2003). Nevertheless, the altered oceanic crust would become dehydrated during subduction, possibly forming

metamorphic eclogite before partial melting. The involvement of the dehydrated oceanic crust is also consistent with the major and trace element characteristics. Partial melting of dehydrated metabasalt (eclogite) typically generates adakitic melts (Defant and Drummond, 1990; Rapp et al., 1991, 2003), which metasomatize peridotite to form silica-deficient pyroxenite (Rapp et al., 1999; Yaxley and Green, 1998; Yaxley, 2000; Sobolev et al., 2005, 2007; Herzberg, 2006). This pyroxenite can be characterized not only by low Mg numbers, high Fe/Mn ratios, no depletion in Nb and Ta but significant depletion in Pb, but also by LREE enrichment and low  $\delta^{18}\text{O}$  values. Although the low Mg numbers and high Fe/Mn ratios for the basalts could be caused by the involvement of delaminated lower continental crust (Gao et al., 2004, 2008; Lustrino, 2005), the low  $\delta^{18}\text{O}$  values preclude this possibility because the lower continental crust cannot be directly overprinted by seawater-hydrothermal alteration to acquire the low  $\delta^{18}\text{O}$  values. Even if the eclogitic composition of the lower crust could be formed by the metamorphic dehydration of the altered oceanic crust during flat subduction below the continental lithosphere, the eclogitic slab would be located below the craton SCLM rather than above the craton SCLM unless the flatly subducted oceanic crust could become the new continental lower crust by just intervention between the continental crust and the craton SCLM.

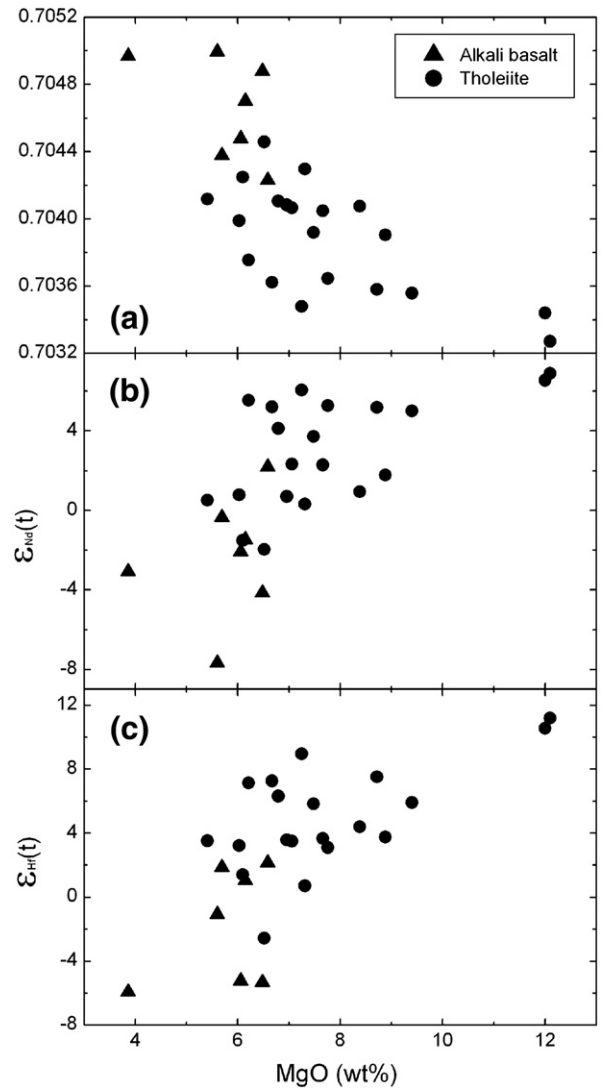


**Fig. 10.** The relationships between MgO concentrations and initial Sr, Nd and Hf isotope ratios for the Wan–Su basalts. (a)  $\epsilon_{\text{Sr}}(t)$  versus MgO; (b)  $\epsilon_{\text{Nd}}(t)$  versus MgO; (c)  $\epsilon_{\text{Hf}}(t)$  versus MgO.

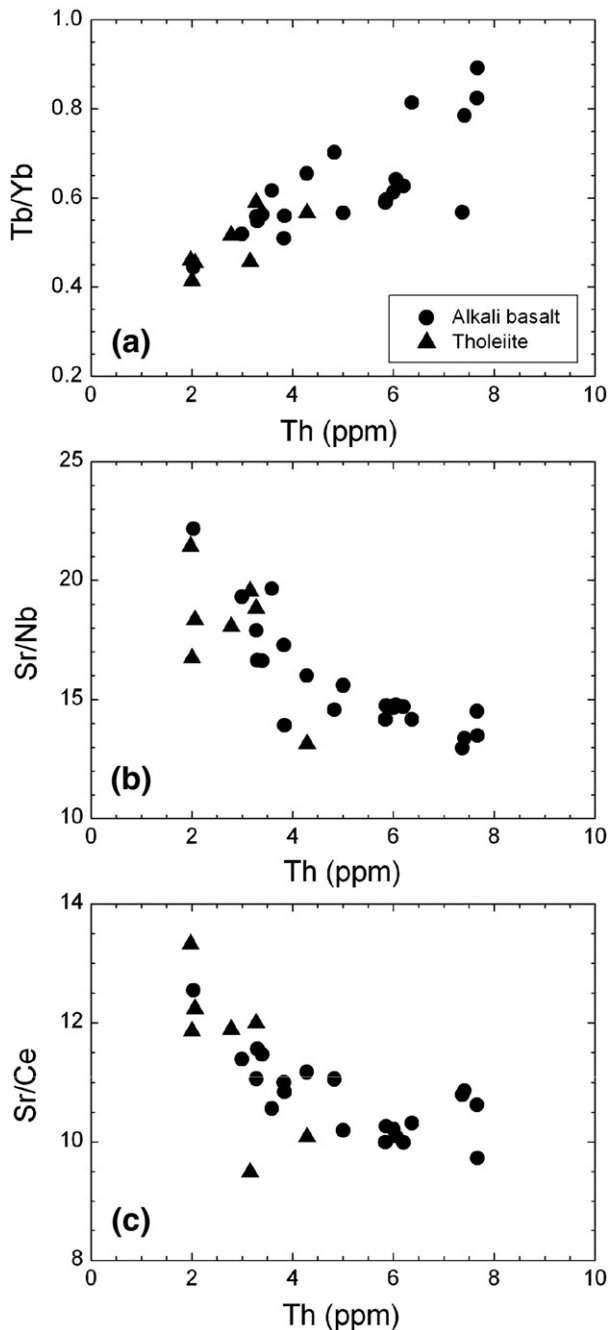


Fig. 11. Abundance ratios of incompatible elements versus Th contents for Cenozoic basalts in Wan-Su. (a) Tb/Yb versus Th for the role of garnet; (b) Sr/Nb versus Th for the role of rutile, and (c) Sr/Ce versus Th for the role of phlogopite.

The tholeiite has the higher  $\delta^{18}\text{O}$  values for phenocrysts, with a smaller variation, than the alkali basalt (Table 6). This suggests less contribution from the low  $\delta^{18}\text{O}$  melts to the tholeiite source than that to the alkali basalt source. Furthermore, the tholeiite has lower MgO, higher  $\text{SiO}_2$ , higher  $I_{\text{Sr}}(t)$ , and lower  $\varepsilon_{\text{Nd}}(t)$  and  $\varepsilon_{\text{Hf}}(t)$  values than the alkali basalt. In particular, it contains the isotopically most enriched component that has an  $I_{\text{Sr}}(t)$  value of 0.705, a  $\varepsilon_{\text{Nd}}(t)$  value of  $-7.67$  and a  $\varepsilon_{\text{Hf}}(t)$  value of  $-5.92$ , corresponding to the oldest Nd and Hf model ages of 1.95 Ga and 1.14 Ga, respectively (Tables 4 and 5). Thus, it is possible that the tholeiite source contains an ancient SCLM component that is at least older than 1.1 Ga. As argued before, however, the craton SCLM cannot be responsible for the isotopically enriched component because of the low MgO contents for the tholeiite. The negative  $\varepsilon_{\text{Nd}}(t)$  and  $\varepsilon_{\text{Hf}}(t)$  values for the tholeiite are

also in discrepancy with its derivation from partial melting of juvenile slab eclogite (Niu and O'Hara, 2003). Instead, the element and isotope characteristics of the tholeiite can be explained by its origin from the silica-excess pyroxenite that formed by metasomatization of the felsic melt. The felsic melt would be derived from partial melting of the dehydrated oceanic metasediment, which is isotopically enriched with high Sr, Nd and Hf elemental contents due to its relative concentration of continent-derived materials (e.g., Sorensen and Grossman, 1993; Plank and Langmuir, 1998; Eisele et al., 2002). As a result, the felsic melt can dominate its budget of Sr–Nd–Hf elements and isotopes over the peridotite, imparting the isotopically enriched signatures to the silica-pyroxenite. The two tholeiite samples (05WD39 and 06SW28) with positive Pb anomalies also have low Ce/Pb ratios of 6.5 to 10.3 (Table S3) as well as low U, Nb and Ta concentrations (Fig. 4d), consistent with involvement of felsic component in their source. In this regard, the tholeiite would originate from the same juvenile SCLM source as the alkali basalt, but its isotopically enriched signatures are inherited from the oceanic metasediment rather than the ancient SCLM. Granulite xenoliths were observed to occur in Cenozoic basalts at Nushan in the Wan–Su area (Yu et al., 2003), with zircon U–Pb ages of  $\sim 2.5$  Ga and  $\sim 1.9$  Ga for protolith and  $140 \pm 4$  to  $117 \pm 5$  Ma for granulitization (Huang et al., 2004). Such a granulite may be a restite after extraction of the felsic melt from the dehydrated oceanic metasediment overlying the dehydrated metabasalt.

### 6.3.3. Preservation of low $\delta^{18}\text{O}$ phenocrysts

The occurrence of low  $\delta^{18}\text{O}$  values for phenocryst minerals in the Wan–Su basalts suggests very short duration of magma residence at mantle depths because rates of O isotope exchange by diffusion are very fast between the minerals and melt at mantle temperatures (Zheng and Fu, 1998; Zheng et al., 1998). Kinetically, relatively long duration is capable of homogenizing the low  $\delta^{18}\text{O}$  melt with the normal upper mantle. Thus, quantitative estimates can be made on timescale of oxygen isotope re-equilibration during basaltic magmatism.

Oxygen isotope re-equilibration could occur when the  $^{18}\text{O}$ -depleted oceanic crust was subducted into the asthenosphere. According to available data from experiments, Zheng et al. (1998) estimated transport rates of 1000 to 2000 m/Ma for oxygen within mafic crust. The timescale required for complete O isotope diffusion re-equilibration can be calculated by the relation (Crank, 1975):  $r \approx \frac{5}{2} \sqrt{Dt}$ , where  $r$  is the effective diffusion radius,  $D$  is the diffusion coefficient and  $t$  is the time. Assuming 6 to 7 km thickness for the subducted oceanic crust, it is estimated that timescales of 1 to 2 Ma would result in complete O isotope re-equilibration between the  $^{18}\text{O}$ -depleted subducted oceanic crust and the normal  $\delta^{18}\text{O}$  asthenosphere. Such short timescales require that the low  $\delta^{18}\text{O}$  melts derived from the dehydrated oceanic crust would not transport through the convective asthenosphere, but directly metasomatize the overlying SCLM. This can explain why the  $^{18}\text{O}$  depletion in the subducted oceanic crust can be preserved and transferred to the erupted basalts.

Clinopyroxene phenocrysts from the Wan–Su basalts have  $\delta^{18}\text{O}$  values of 4.42‰ to 5.70‰, generally lower than the normal upper mantle values of  $5.6 \pm 0.2$ ‰ (Fig. 6a). Olivine phenocryst  $\delta^{18}\text{O}$  values vary widely from 4.00‰ to 5.91‰, but mostly fall within the range of the normal upper mantle values of  $5.2 \pm 0.2$ ‰ (Fig. 6b). Obviously, there is O isotope disequilibrium between clinopyroxene and olivine. It is known that the rates of O diffusion in minerals are principally controlled by crystalline structure and diffusion medium (Zheng and Fu, 1998). In particular, rates of O diffusion in minerals under hydrothermal conditions are significantly greater than those under anhydrous conditions (Fig. 6c). By taking the grain radii of clinopyroxene and olivine (200  $\mu\text{m}$ ) as effective diffusion radii, the timescales of achieving O isotope re-equilibration by diffusion exchange at temperatures of basaltic magma emplacement ( $\sim 1200$  °C) can be calculated (Fig. 6d). The results suggest that rates of O diffusion in

clinopyroxene are close to those in olivine and that under both anhydrous and hydrothermal conditions, the timescales required for diffusion re-equilibration across both minerals are 1 ka and 0.01 ka, respectively (Fig. 6d). This indicates that the maximum timescale for melting, transport and eruption would probably be less than 1 ka. In that case, the low  $\delta^{18}\text{O}$  values inherited from the source are able to be preserved in clinopyroxene and few olivine phenocrysts.

## 7. Petrogenetic model

Radiogenic isotope studies indicate that both depleted and enriched mantle components contribute to the production of continental basalts. In particular, SCLM has been suggested to be the potential source for many continental basalts (e.g., Ellam and Cox, 1989; Gallagher and Hawkesworth, 1992; Anderson, 1994; Silver et al., 2006). SCLM can form by lateral accretion of subarc mantle to continental margin via arc-continent collision (Jordan, 1988; Lee, 2006; Pearson and Wittig, 2008), or by high-degree melting in a mantle plume (Boyd, 1989; Arndt et al., 2002; Griffin et al., 2003). It may also form by subcontinental processes through flat subduction and underplating of oceanic lithosphere (Helmstaedt and Schulze, 1989), or by underplating of the asthenosphere along lithospheric rifting (Zheng et al., 2006). The subarc mantle is commonly infertile and thus refractory due to the extraction of arc basaltic melts, but it could become highly fertile if no melt was immediately extracted following influx of aqueous fluid. Petrologically, the infertile SCLM is principally coupled with extraction of the arc basalt-, OIB- or MORB-type crustal melts, leaving the highly refractory residues as the craton SCLM. If the fertile SCLM did not undergo melt extraction, it is probably decoupled with the overlying crust with respect to the time of chemical differentiation. In addition, the dehydrated oceanic crust would be returned to the asthenospheric mantle via the subduction of oceanic lithosphere, giving rise to oceanic island basalts (Hofmann and White, 1982).

The isotopically most depleted component of the Wan–Su basalts occurs in the alkali basalt and has an  $I_{\text{Sr}}(t)$  ratio of 0.703, a  $\varepsilon_{\text{Nd}}(t)$  value of 6.89 and a  $\varepsilon_{\text{Hf}}(t)$  value of 11.19. It corresponds to the youngest Nd and Hf model ages of 293 Ma and 267 Ma, respectively (Tables 4 and 5). This component requires the involvement of relatively depleted and thus young SCLM (Late Paleozoic–Early Mesozoic). Only the juvenile SCLM is capable of generating the basaltic melts with the isotopic compositions similar to those derived from the asthenosphere. This is consistent with Mesozoic–Cenozoic  $\text{Os}$  model ages ( $T_{\text{RD}}$  for time of Re depletion) for spinel peridotite xenoliths of Cenozoic basalts in the Wan–Su area (recalculated by Xu et al., 2008 from whole-rock Re–Os isotope data of Reisberg et al., 2005). On the other hand, there are gradual variations in element abundances and isotope compositions from the alkalic to tholeiitic basalts. This can be caused by variable proportions of mixing between the near-solidus melts that were derived from the isotopically depleted silica-deficient pyroxenite and the isotopically enriched silica-pyroxenite, respectively. In particular, the felsic melt from the dehydrated oceanic metasediment dominates its composition of radiogenic Sr, Nd and Hf isotopes over the metasomatized peridotite, imparting the isotopically enriched signatures to the silica-excess pyroxenite that looks like the ancient SCLM.

The trace element signatures in the Wan–Su basalts provide at least three constraints on their magma source. First, garnet was present as a residual phase during partial melting, but rutile and phlogopite were dissolved. Second, the source was considerably dehydrated, resulting in the depletion of water-soluble elements (e.g., Rb and Pb) but no depletion of water-insoluble elements (e.g., Nb and Ta). Third, the direct contribution from partial melting of either the asthenosphere or the craton SCLM is insignificant. Although the Wan–Su basalts mostly exhibit negative Rb and Pb anomalies relative to their neighbouring elements, they have less positive Sr anomalies and weaker negative Pb

anomalies than OIB (Fig. 4c and d). Furthermore, they show a strongly positive correlation between Sr and Nb (Fig. 9a), indicating relatively low extents to which the source was dehydrated prior to melting. Therefore, the geochemistry of these basalts requires a different source from both MORB and OIB. On the other hand, the preservation of low  $\delta^{18}\text{O}$  phenocrysts in the alkali basalt indicates immediate reaction of low  $\delta^{18}\text{O}$  adakitic melts with the overlying peridotite, without transportation through the asthenosphere.

Thus, we assume low-angle subduction of the Pacific Plate beneath the Eurasian continent during the Early Mesozoic (Li and Li, 2007), which may have brought the dehydrated oceanic crust as a slab below the ancient SCLM in east-central China. It is the low-angle subduction that would have delaminated the lower part of the ancient SCLM into the asthenosphere on one hand and transforming the mantle wedge overlying the subducted oceanic crust to the juvenile SCLM on the other hand (Fig. 12a). The dehydrated oceanic basalt would initially become eclogite (s.l.) during the subduction, and then undergo partial melting to generate the adakitic melt. In contrast, the dehydrated metasediment overlying the eclogite slab would be partially molten to generate the felsic melt. Subsequently, the adakitic and felsic melts would ascend rapidly and react with the overlying juvenile SCLM peridotite to form the silica-deficient and silica-excess pyroxenites, respectively, during the Late Mesozoic. Thus the juvenile SCLM is

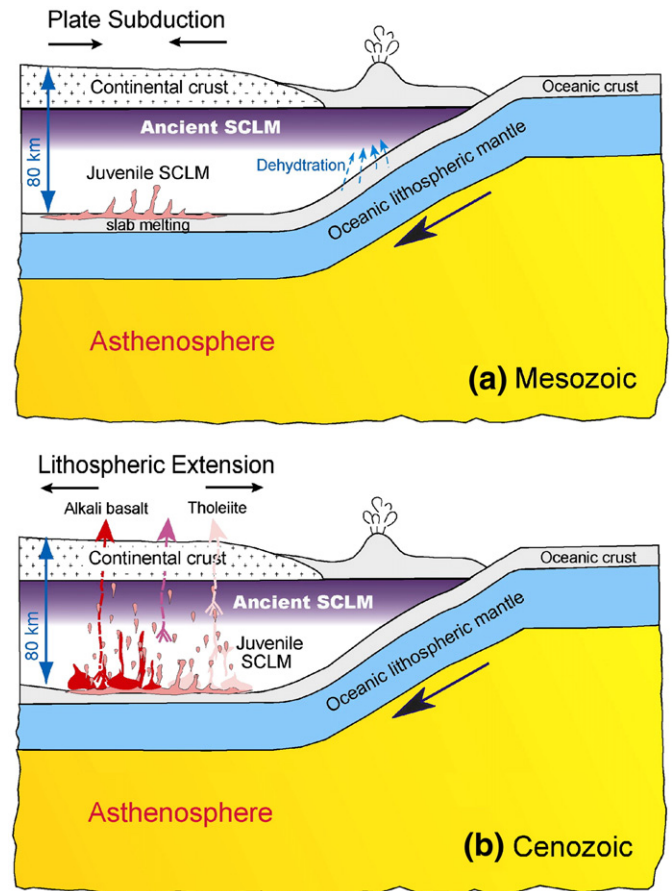


**Fig. 12.** Cartoon illustrating a petrogenetic model of oceanic crust-lithospheric mantle interaction for Cenozoic continental basalts in east-central China. (a) Early Mesozoic subduction of the oceanic crust transforms the mantle wedge to the juvenile SCLM, leaving the thinned ancient SCLM beneath continental crust. Very small amounts of slab melts derived from dehydrated oceanic crust metasomatize the overlying juvenile SCLM peridotite to form pyroxenites during the Late Mesozoic. (b) Cenozoic melting of silica-deficient to silica-excess pyroxenites underlying the juvenile SCLM occurs, resulting in alkalic to tholeiitic basalts. Note that the spatial relationships between the ancient and juvenile SCLMs and between the alkalic and tholeiitic basalts are strictly schematic, possibly with gradual thinning of the ancient SCLM at the locality close to the subduction zone.

bracketed by the ancient SCLM above and the pyroxenites below. Finally, partial melting of the pyroxenites was triggered in far backarc extension settings in response to the Cenozoic subduction of the Pacific Plate beneath the eastern part of the Eurasian continent, generating the alkalic to tholeiitic basalts (Fig. 12b).

The mechanism of craton SCLM thinning in the North China Block during the Phanerozoic may be related to the thermal/chemical erosion of the craton SCLM (e.g., Griffin et al., 1998; Xu, 2001) or the delamination of the lower crust (e.g., Gao et al., 2002; Wu et al., 2003). The difference between these two models lies in the tectonic trigger and the amount and rate of removed materials. The thermal/chemical erosion envisages gradual removal of the craton SCLM by asthenosphere upwelling, whereas the delamination presumes massive removal of the eclogite-facies lower crust and its underlying craton SCLM by gravitational sinking. However, the tectonic trigger for the thinning still remains elusive (e.g., Wilde et al., 2003; Zhang et al., 2003; Deng et al., 2004; Gao et al., 2004; Wu et al., 2005; Zheng and Zhang, 2007). As stated in the introduction, the North China Block was subducted by the Siberian Plate during the Paleozoic, by the South China Block during the Late Paleozoic to Early Mesozoic, and by the Pacific Plate during the Mesozoic. For the South China Block, on the other hand, it was only subducted by the Indochina Block during the Late Paleozoic to Early Mesozoic, and by the Pacific Plate during the Mesozoic. In this regard, the Early Mesozoic low-angle subduction of the Pacific Plate may have played a major role of thinning the ancient SCLM in the eastern part of China. Thus, subduction erosion may be an alternative mechanism for the ancient SCLM thinning. This can be achieved by lateral convection of the asthenosphere above the subducting oceanic crust, with preferential removal of orogenic roots (lithospheric keels) in response to the rotated subduction of the Pacific Plate during the Early Cretaceous (Zhao et al., 2007; Zheng, 2008).

Although this study does not consider the ancient SCLM as a source for the tholeiite, our petrogenetic model suggests that the SCLM beneath the east-central China was stratified prior to the Cenozoic magmatism of continental basalts, with the ancient SCLM overlying the juvenile SCLM. Geochemical studies of peridotite xenoliths in Cenozoic basalts at Nushan and Late Mesozoic basalts at Jünan also favour the possibility of SCLM stratification in east-central China (Xu and Bodinier, 2004; Ying et al., 2006). Re-Os isotope studies of peridotite xenoliths from the northeastern edge of the South China Block do indicate the existence of Late Mesoproterozoic SCLM (Zhang et al., 2008) and Middle Paleoproterozoic SCLM (Jin et al., 2004; Reisberg et al., 2005; Yuan et al., 2007). A similar SCLM stratification was also suggested for the North China Block based on geochemical studies of Cenozoic basalts (Xu et al., 2004). Therefore, the SCLM stratification is present not only in east-central China but also in North China. This lends support to the hypothesis that majority of the ancient SCLM was delaminated by the subduction erosion and then dissolved into the asthenosphere. Such a tectonic process would result in not only the massive lithospheric thinning but also the intensive mantle heterogeneity. In this regard, it is intriguing to examine how the ancient SCLM was metasomatized by basaltic melts derived from the juvenile SCLM during the shallow melt-peridotite reaction due to the asthenosphere-lithosphere interaction.

Both adakitic and felsic melts derived from the dehydrated oceanic crust are suggested to serve as metasomatized agents for the formation of silica-deficient and silica-excess pyroxenites, respectively. This is the deep melt-peridotite reaction due to interaction between the oceanic crust and the juvenile SCLM. An assumption behind this suggestion is that the isotopically enriched component in the pyroxenites originates from the dehydrated metasediment overlying the dehydrated metabasalt (eclogite). This is consistent with the observation of Huang et al. (2004) that the granulite xenoliths in the Nushan basalts have initial  $^{87}\text{Sr}/^{86}\text{Sr}$  ratios of 0.7040 to 0.7071 and  $\epsilon_{\text{Nd}}(t)$  values of  $-33.9$  to  $-23.4$  at  $t = 140$  Ma. Pyroxenite xenoliths from Cenozoic basalts at Hannuoba in the northern edge of the North China

Block are isotopically more enriched than the peridotite xenoliths (Liu et al., 2004; Rudnick et al., 2004). Therefore, the juvenile SCLM is underlain by the pyroxenites. Furthermore, the granulite and eclogite are the restites after extraction of the adakitic and felsic melts, respectively. In this context, granulite xenoliths in continental basalts would be located beneath the juvenile SCLM rather than the continental crust. Thus, they are not samples of the deep lower crust. They also differ from terrane granulites in that the former underwent melt extraction whereas the latter only experienced dehydration metamorphism.

Recent studies of seismic tomography suggest the presence of flat slab below the eastern part of the China continent (Huang and Zhao, 2006), but in much deeper mantle transition zone rather than on the top of the asthenosphere. This implies that the SCLM and the subducted Pacific slab are separated by asthenosphere at present. If the slab melting could occur within the asthenosphere and the low  $\delta^{18}\text{O}$  melts would ascend through the convective asthenosphere, the low  $\delta^{18}\text{O}$  signature would be homogenized to the normal upper mantle  $\delta^{18}\text{O}$  values. This is in discrepancy with the preservation of low  $\delta^{18}\text{O}$  phenocrysts in the Wan–Su basalts. Instead, the low  $\delta^{18}\text{O}$  melts would metasomatize the overlying juvenile SCLM peridotite to form the pyroxenites without transportation through the convective asthenosphere. Therefore, the seismically imaged position of flat slab may be a result of the gravitational sinking after extraction of slab melts from the dehydrated oceanic crust. In particular, it is likely that the formation of the adakitic melt temporally marks the onset of the gravitational sinking of high-density eclogite and its underlying oceanic lithospheric mantle into the asthenosphere. Although no chronometric dates are available for pyroxenite xenoliths in the Cenozoic continental basalts in eastern China, zircon U–Pb dating for the granulite xenoliths at Nushan in the Wan–Su area gave ages of  $140 \pm 4$  to  $117 \pm 5$  Ma for melt extraction during granulitization (Huang et al., 2004). In this regard, the slab melting at about 140 Ma may signify a switch from the low-angle subduction of oceanic lithosphere beneath the ancient SCLM to the high-angle subduction beneath the juvenile SCLM through slab roll-back and retreat. Such a switch may be caused by a change in the subduction direction and rate of Pacific Plate beneath the Eurasian continent during the Early Cretaceous (Sun et al., 2007; Zheng, 2008). It would not only postdate the delamination of the craton SCLM beneath the continental crust, but also predate the gravitational sinking of eclogite slab beneath the juvenile SCLM toward the mantle transition zone. The slab sinking would leave space for lateral emplacement of the asthenosphere between the juvenile SCLM and the sinking oceanic lithosphere. Thus, it is intriguing to examine whether there was the deep melt-peridotite reaction, or only the thermal baking to the juvenile SCLM, during this period of asthenosphere-lithosphere interaction. In addition, it remains to be tested whether this switch marks the onset of the TanLu fault in eastern China, with the stretch-induced delamination of lithospheric keels and high-Mg adakitic magmatism (Huang et al., 2008).

## 8. Conclusions

Cenozoic continental basalts from east-central China display geochemical features that cannot be explained by crustal contamination, fractional crystallization and different degrees of partial melting alone. Instead, they are best accounted for by near-solidus partial melting of the same juvenile SCLM that is composed of silica-deficient and silica-excess pyroxenites. Differences in element and isotope compositions between the alkalic and tholeiitic basalts can be explained by differences in the two types of pyroxenites and thus in their metasomatizing agents (adakitic versus felsic melts). In particular, the felsic melt was presumably derived from partial melting of dehydrated oceanic metasediment, dominating its composition of Sr, Nd and Hf elements and isotopes in the silica-excess pyroxenite. Preservation of low  $\delta^{18}\text{O}$  phenocrysts suggests that adakitic melts

from dehydrated low  $\delta^{18}\text{O}$  oceanic metabasalt were not transported through the convective asthenosphere, but directly metasomatized the overlying juvenile SCLM. Oxygen isotope disequilibrium between olivine and clinopyroxene provides a quantitative constraint on the maximum timescale that is less than 1 ka for melting, transport and eruption during basaltic magmatism.

A model of oceanic crust–lithospheric mantle interaction is proposed for petrogenesis of the continental basalts, in which only the juvenile SCLM would be involved without material contribution from the ancient SCLM and the asthenosphere. The low-angle subduction of the Pacific Plate during the Early Mesozoic beneath the continental edge of eastern China is suggested to play a key role in thinning of the continental lithosphere in the North China Block. This would have not only delaminated the craton SCLM into the asthenosphere resulting in the mantle heterogeneity, but would have also transformed the mantle wedge to the juvenile SCLM. Very small amounts of the adakitic and felsic melts would be respectively generated from the dehydrated oceanic metabasalt and metasediment during the Late Mesozoic. Such slab melts would ascend rapidly, metasomatizing the overlying the juvenile SCLM peridotite to form isotopically depleted silica-deficient and enriched silica-excess pyroxenites, respectively. This yields a juvenile SCLM beneath the thinned ancient SCLM, with the pyroxenites at the bottom. Because of the lithospheric rifting in the Cenozoic, near-solidus partial melting of the pyroxenites generates the alkalic to tholeiitic basalts with OIB-like features of trace elements and radiogenic isotopes. As a result, the continental basalts were derived from the products of deep melt–peridotite reaction that is petrogenetically coupled with the thinning of the ancient SCLM and the asthenosphere–lithosphere interactions.

## Acknowledgments

This study was supported by funds from the Natural Science Foundation of China (90714009) and the Chinese Academy of Sciences (KZCX2-YW-Q08). Thanks are due to T.-S. Gao and Y.-B. Wu for their assistance during the field trip, to X.P. Zha and B.C. Ding for their assistance with O isotope analyses, and to F.K. Chen and Y.H. Yang for their assistance with radiogenic isotope analyses. We are grateful to T. Furman, A.C. Kerr, Y.G. Xu and one anonymous reviewer for their comments on earlier versions of the manuscript that greatly helped improvement of the presentation.

## Appendix A. Supplementary data

Supplementary data associated with this article can be found, in the online version, at doi:10.1016/j.lithos.2009.01.006.

## References

- Anderson, D.L., 1994. Lithosphere and flood basalts. *Nature* 367, 226–226.
- Anderson, D.L., 2005. Large igneous provinces, delamination, and fertile mantle. *Elements* 1, 271–275.
- Anhui BGM (Bureau of Geology and Mineral Resources), 1978. Regional Geology Records of Anhui Province (in Chinese). Geological Publishing House, Beijing. 189–190 pp.
- Arndt, N.T., Albarède, F., Lewin, E., 2002. Strange partners: formation and survival of continental crust and lithospheric mantle. *Geological Society Special Publication* 199, 91–103.
- Barry, T.L., Saunders, A.D., Kempton, P.D., Windley, B.F., Pringle, M.S., Dorjnamjaa, D., Saandar, S., 2003. Petrogenesis of Cenozoic basalts from Mongolia: evidence for the role of asthenospheric versus metasomatized lithospheric mantle sources. *Journal of Petrology* 44, 55–91.
- Basu, A.R., Junwen, W., Wanking, H., Guanghong, X., Tatsumoto, M., 1991. Major element, REE, and Pb, Nd and Sr isotopic geochemistry of Cenozoic volcanic rocks of eastern China: implications for their origin from suboceanic-type mantle reservoirs. *Earth and Planetary Science Letters* 105, 149–169.
- Bizzarro, M., Baker, J.A., Ulfbeck, D., 2003. A new digestion and chemical separation technique for rapid and highly reproducible determination of Lu/Hf and Hf isotope ratios in geological materials by MC-ICP-MS. *Geostandards Newsletter* 27, 133–145.
- Boyd, F.R., 1989. Compositional distinction between oceanic and cratonic lithosphere. *Earth and Planetary Science Letters* 96, 15–26.
- Burke, K.C., Wilson, J.T., 1976. Hot spots on the Earth surface. *American Journal of Science* 21, 46–57.
- Campbell, I.H., Griffiths, R.W., 1990. Implications of mantle plume structure for the evolution of flood basalts. *Earth and Planetary Science Letters* 99, 79–93.
- Caroff, M., Maury, R.C., Cotton, J., Clément, J.P., 2000. Segregation structures in vapor differentiated basaltic flows. *Bulletin of Volcanology* 62, 171–187.
- Chen, D.G., Peng, Z.C., 1988. K–Ar ages, Nd and Sr isotopic characteristics of some Cenozoic volcanic rocks in Anhui–Jiangsu. *Acta Petrologica Sinica* (in Chinese with English abstract) 4, 3–12.
- Chen, F.K., Hegner, E., Todt, W., 2000. Zircon ages, Nd isotopic and chemical compositions of orthogneisses from the Black Forest, Germany – evidence for a Cambrian magmatic arc. *International Journal of Earth Science* 88, 791–802.
- Chen, B., Jahn, B.-m., Ye, K., Liu, J.B., 2002a. Cogenetic relationship of the Yangkou gabbro-to-granite unit, Su-Lu terrane, eastern China, and implications for UHP metamorphism. *Journal of the Geological Society London* 159, 457–467.
- Chen, F.K., Siebel, W., Satir, M., Terzioglu, N., Saka, K., 2002b. Geochronology of the Karadere basement (NW Turkey) and implications for the geological evolution of the Istanbul zone. *International Journal of Earth Science* 91, 469–481.
- Chen, Y., Zhang, Y.X., Graham, D., Su, S.G., Deng, J.F., 2007. Geochemistry of Cenozoic basalts and mantle xenoliths in Northeast China. *Lithos* 96, 108–126.
- Chiba, H., Chacko, T., Clayton, R.N., Goldsmith, J.R., 1989. Oxygen isotope fractionations involving diopside, forsterite, magnetite, and calcite: application to geothermometry. *Geochimica et Cosmochimica Acta* 53, 2985–2995.
- Chung, S.-L., 1999. Trace element and isotope characteristics of Cenozoic basalts around the Tanlu Fault with implications for the eastern plate boundary between north and south China. *The Journal of Geology* 107, 301–312.
- Chung, S.-L., Sun, S.-s., Tu, K., Chen, C.-H., Lee, C.-y., 1994. Late Cenozoic basaltic volcanism around the Taiwan Strait, SE China: product of lithosphere–asthenosphere interaction during continental extension. *Chemical Geology* 112, 1–20.
- Cong, B.L., 1996. Ultrahigh-pressure Metamorphic rocks in the Dabieshan-Sulu Region of China. Science Press, Beijing. 224 pp.
- Crank, J., 1975. *The Mathematics of Diffusion*. Clarendon Press, Oxford.
- Dalpe, C., Baker, D.R., 2000. Experimental investigation of large ion lithophile element, high field strength element and rare earth element partitioning between calcic amphibole and basaltic melt: the effects of pressure and oxygen fugacity. *Contributions to Mineralogy and Petrology* 140, 233–250.
- Defant, M.J., Drummond, M.S., 1990. Derivation of some modern arc magmas by melting of young subducted lithosphere. *Nature* 347, 662–665.
- Deng, J.F., Zhao, H.L., Guo, Z.F., Luo, Z.H., Mo, X.X., 1998. Mantle plumes and lithosphere motion in East Asia. In: Flower, M.F.J., Chung, S.-L., Lo, C.-H., Lee, T.-Y. (Eds.), *Mantle Dynamics and Plate Interactions in East Asia*. American Geophysical Union Geodynamics Series, vol. 27, pp. 59–65.
- Deng, J.F., Mo, X.X., Zhao, H.L., Wu, Z.X., Luo, Z.H., Su, S.G., 2004. A new model for the dynamic evolution of Chinese lithosphere: ‘continental roots-plume tectonics’. *Earth-Science Review* 65, 223–275.
- DePaolo, D.J., 1988. *Neodymium Isotope Geochemistry: An Introduction*. Springer-Verlag, Berlin. 189 pp.
- DePaolo, D.J., Daley, E.E., 2000. Neodymium isotopes in basalts of the Southwest Basin and Range and lithospheric thinning during continental extension. *Chemical Geology* 169, 157–185.
- Dostal, J., Dupuy, C., Zhai, M.Z., Zhi, X.C., 1988. Geochemistry and origin of Pliocene alkali basaltic lavas from Anhui–Jiangsu, eastern China. *Geochemical Journal* 22, 165–176.
- Eiler, J.M., 2001. Oxygen isotope variations of basaltic lavas and upper mantle rocks. *Reviews in Mineralogy & Geochemistry* 43, 319–364.
- Eiler, J.M., Farley, K.A., Valley, J.W., Hauri, E., Craig, H., Hart, S., Stolper, E.M., 1996. Oxygen isotope variations in ocean island basalt phenocrysts. *Geochimica et Cosmochimica Acta* 61, 2281–2293.
- Eisele, J., Sharma, M., Galer, S.J.G., Blichert-Toft, J., Devey, C.W., Hofmann, A.W., 2002. The role of sediment recycling in EM-1 inferred from Os, Pb, Hf, Nd, Sr isotope and trace element systematics of the Pitcairn hotspot. *Earth and Planetary Science Letters* 196, 197–212.
- Ellam, R.M., Cox, K.G., 1989. A Proterozoic lithospheric source for Karoo magmatism: evidence from the Nuanetsi picrites. *Earth and Planetary Science Letters* 92, 207–218.
- Fan, Q.C., Hooper, P.R., 1991. The Cenozoic basaltic rocks of eastern China: petrology and chemical composition. *Journal of Petrology* 32, 765–810.
- Fan, W.M., Zhang, H.F., Baker, J., Javis, K.E., Mason, P.R.D., Menzies, M.A., 2000. On and off the North China craton: where is the Archaean keel? *Journal of Petrology* 41, 933–950.
- Fitton, J.G., 2007. The OIB paradox. In: Foulger, G.R., Jurdy, D.M. (Eds.), *Plates, Plumes, and Planetary Processes*. Geological Society of America Special Paper, vol. 430, pp. 387–412.
- Fitton, J.G., Saunders, A.D., Norry, M.J., Hardarson, B.S., Taylor, R.N., 1997. Thermal and chemical structure of the Iceland plume. *Earth and Planetary Science Letters* 153, 197–208.
- Flower, M.F.J., Tamaki, K., Hoang, N., 1998. Mantle extrusion: a model for dispersed volcanism and Dupal-like asthenosphere in East Asia and the Western Pacific. In: Flower, M.F.J., Chung, S.-L., Lo, C.-H., Lee, T.-Y. (Eds.), *Mantle Dynamics and Plate Interactions in East Asia*. American Geophysical Union Geodynamics Series, vol. 27, pp. 67–88.
- Foley, S.F., Barth, M.G., Jenner, G.A., 2000. Rutile/melt partition coefficients for trace elements and assessment of the influence of rutile on the trace element characteristics of subduction zone magmas. *Geochimica et Cosmochimica Acta* 64, 933–938.
- Gallagher, K., Hawkesworth, C., 1992. Dehydration melting and the generation of continental flood basalts. *Nature* 358, 57–59.

- Gao, S., Rudnick, R.L., Carlson, R.W., McDonough, W.F., Liu, Y.S., 2002. Re–Os evidence for replacement of ancient mantle lithosphere beneath the North China Craton. *Earth and Planetary Science Letters* 198, 307–322.
- Gao, S., Rudnick, R.L., Yuan, H.-L., Liu, X.-M., Liu, Y.-S., Xu, W.-L., Ling, W.-L., Ayers, J., Wang, X.-C., Wang, Q.-H., 2004. Recycling lower continental crust in the North China craton. *Nature* 432, 892–897.
- Gao, S., Rudnick, R.L., Xu, W.L., Yuan, H.L., Liu, Y.S., Puchtel, I., Liu, X., Huang, H., Wang, X.R., 2008. Recycling deep cratonic lithosphere and generation of intraplate magmatism. *Earth and Planetary Science Letters* 270, 41–53.
- Gautason, B., Muehlenbachs, K., 1998. Oxygen isotopic fluxes associated with high-temperature processes in the rift zones of Iceland. *Chemical Geology* 145, 275–286.
- Gibson, S.A., Thompson, R.N., Dickin, A.P., Leonardos, O.H., 1996. High-Ti and low-Ti mafic potassic magmas: key to plume–lithosphere interactions and continental flood basalt genesis. *Earth and Planetary Science Letters* 141, 325–341.
- Goff, F.E., 1996. Vesicle cylinders in vapor-differentiated basalt flows. *Journal of Volcanology and Geothermal Research* 71, 167–185.
- Green, T.H., 1980. Island arc and continent-building magmatism; a review of petrogenetic models based on experimental petrology and geochemistry. *Tectonophysics* 63, 367–385.
- Griffin, W.L., Zhang, A., O'Reilly, S.Y., Ryan, C.G., 1998. Phanerozoic evolution of the lithosphere beneath the Sino–Korean craton. In: Flower, M., Chung, S.L., Lo, C.H., Lee, Y.Y. (Eds.), *Mantle Dynamics and Plate Interactions in East Asia*. American Geophysical Union Geodynamics Series, vol. 27, pp. 107–126.
- Griffin, W.L., Pearson, N.J., Belousova, E., Jackson, S.E., van Acherbergh, E., O'Reilly, S.Y., Shee, S.R., 2000. The Hf isotope composition of cratonic mantle: LAM-MC-ICPMS analysis of zircon megacrysts in kimberlites. *Geochimica et Cosmochimica Acta* 64, 133–147.
- Griffin, W.L., O'Reilly, S.Y., Abe, N., Aulbach, S., Davies, R.M., Pearson, N.J., Doyle, B.J., Kivi, K., 2003. The origin and evolution of Archean lithospheric mantle. *Precambrian Research* 127, 19–41.
- Hawkesworth, C.J., Hergt, J.M., Ellam, R.M., McDermott, F., 1991. Element fluxes associated with subduction related magmatism. *Philosophical Transaction of Royal Society A335*, 393–405.
- Helmstaedt, H., Schulze, D.J., 1989. Southern African kimberlites and their mantle sample; implications for Archean tectonics and lithosphere evolution. *Geological Society of Australia, Special Publication* 14, 358–368.
- Herzberg, C., 2006. Petrology and thermal structure of the Hawaiian plume from Mauna Kea volcano. *Nature* 444, 605–609.
- Hirose, K., Kushiro, I., 1993. Partial melting of dry peridotites at high pressures: determinations of compositions of melts segregated from peridotite using aggregates of diamond. *Earth and Planetary Science Letters* 114, 477–489.
- Hirschmann, M.M., Kogiso, T., Baker, M., Stolper, E.M., 2003. Alkaline magmas generated by partial melting of garnet pyroxenite. *Geology* 31, 481–484.
- Hofmann, A.W., 1997. Mantle geochemistry: the message from oceanic volcanism. *Nature* 385, 219–229.
- Hofmann, A.W., White, W.M., 1982. Mantle plumes from ancient oceanic crust. *Earth and Planetary Science Letters* 57, 421–436.
- Hofmann, A.W., Feigenson, M.D., Raczek, I., 1984. Case studies on the origin of basalt. III. Petrogenesis of the Mauna Ulu eruption Kilauea, 1969–1971. *Contributions to Mineralogy and Petrology* 88, 24–35.
- Hofmann, A.W., Jochum, K.P., Seufert, M., White, W.M., 1986. Nb and Pb in oceanic basalts: new constraints on mantle evolution. *Earth and Planetary Science Letters* 79, 33–45.
- Huang, J.L., Zhao, D.P., 2006. High-resolution mantle tomography of China and surrounding regions. *Journal of Geophysical Research* 111, B09305. doi:10.1029/2005JB004066.
- Huang, X.L., Xu, Y.G., Liu, D.Y., 2004. Geochronology, petrology and geochemistry of the granulite xenoliths from Nushan, east China: implication for a heterogeneous lower crust beneath the Sino–Korean Craton. *Geochimica et Cosmochimica Acta* 68, 127–149.
- Huang, J., Zheng, Y.-F., Zhao, Z.-F., Wu, Y.-B., Zhou, J.-B., Liu, X.M., 2006. Melting of subducted continent: element and isotopic evidence for a genetic relationship between Neoproterozoic and Mesozoic granitoids in the Sulu orogen. *Chemical Geology* 229, 227–256.
- Huang, F., Li, S.G., Dong, F., He, Y.S., Chen, F.K., 2008. High-Mg adakitic rocks in the Dabie orogen, central China: Implications for foundering mechanism of lower continental crust. *Chemical Geology* 255, 1–13.
- Humayun, M., Qin, L., Norman, M.D., 2004. Geochemical evidence for excess iron in the mantle beneath Hawaii. *Science* 306, 91–94.
- Jahn, B.-m., 1998. Geochemical and isotopic characteristics of UHP eclogites and ultramafic rocks of the Dabie orogen: implications for continental subduction and collisional tectonics. In: Hacker, B.R., Liou, J.G. (Eds.), *When Continents Collide: Geodynamics and Geochemistry of Ultrahigh-pressure Rocks*. Kluwer Academic Publishers, Dordrecht, pp. 203–239.
- Jin, Y.B., Zhi, X.C., Meng, Q., Gao, T.S., Peng, Z.C., 2004. Re–Os dating of the Raobazhai ultramafic massif in North Dabie. *Chinese Science Bulletin* 49, 508–513.
- Jordan, T.H., 1988. Structure and formation of the continental tectosphere. *Journal of Petrology, Special Lithosphere Issue* 11–13.
- Keshav, S., Gudfinnsson, G.H., Sen, G., Fei, Y.W., 2004. High-pressure melting experiments on garnet clinopyroxenite and the alkalic to tholeiitic transition in ocean island basalts. *Earth and Planetary Science Letters* 223, 365–379.
- Kinzler, R.J., 1997. Melting of mantle peridotite at pressure approaching the spinel to garnet transition: application to mid-ocean ridge petrogenesis. *Journal of Geophysical Research* 102, 853–874.
- Kleinhanns, I.C., Kleinhanns, I.C., Kreissig, K., Kamber, B.S., Meisel, T., Nagler, T.F., Kramers, J.D., 2002. Combined chemical separation of Lu, Hf, Sm, Nd, and REEs from a single rock digest: precise and accurate isotope determinations of Lu–Hf and Sm–Nd using multicollector-ICPMS. *Analytical Chemistry* 74, 67–73.
- Klemme, S., Blundy, J.D., Wood, B.D., 2002. Experimental constraints on major and trace element partitioning during partial melting of eclogite. *Geochimica et Cosmochimica Acta* 66, 3109–3123.
- Kogiso, T., Hirschmann, M.M., 2006. Partial melting experiments of biminerally eclogite and the role of recycled mafic oceanic crust in the genesis of ocean island basalts. *Earth and Planetary Science Letters* 249, 188–199.
- Kogiso, T., Hirschmann, M.M., Frost, D.J., 2003. High-pressure partial melting of garnet pyroxenite: possible mafic lithologies in the source of ocean island basalts. *Earth and Planetary Science Letters* 216, 603–617.
- Kushiro, I., 2001. Partial melting experiments on peridotite and origin of mid-ocean ridge basalts. *Annual Review of Earth and Planetary Sciences* 29, 71–107.
- Langmuir, C.H., Klein, E.M., Plank, T., 1992. Petrological systematics of mid-ocean ridge basalts: constraints on melt generation beneath ocean ridge. *American Geophysical Union Geophysical Monograph Series* 71, 81–180.
- LaTourrette, T.Z., Hervig, R.L., Holloway, J.R., 1995. Trace element partitioning between amphibole, phlogopite, and basanite melt. *Earth and Planetary Science Letters* 135, 13–30.
- Le Bas, M.J., Le Maitre, R.W., Streckeisen, A., Zanettin, B., 1986. A chemical classification of volcanic rocks based on the total alkali–silica diagram. *Journal of Petrology* 27, 745–750.
- Lee, C.-T.A., 2006. Geochemical/petrologic constraints on the origin of cratonic mantle. In: Benn, K., Mareschal, J.-C., Condie, K.C. (Eds.), *Archean Geodynamics and Environments*. American Geophysical Union Monograph, pp. 89–114. Washington.
- Le Fevre, B., Pin, C., 2001. An extraction chromatography method for Hf separation prior to isotopic analysis using multiple collection ICP-mass spectrometry. *Analytical Chemistry* 73, 2453–2460.
- Li, Z.X., Li, X.H., 2007. Formation of the 1300-km-wide intracontinental orogen and postorogenic magmatic province in Mesozoic South China: a flat-slab subduction model. *Geology* 35, 179–182.
- Li, S.C., Jagoutz, E., Lo, C.-H., Chen, Y.Z., Li, Q.L., Xiao, Y.L., 1999. Sm/Nd, Rb/Sr, and <sup>40</sup>Ar/<sup>39</sup>Ar isotopic systematics of the ultrahigh-pressure metamorphic rocks in the Dabie–Sulu belt, Central China: a retrospective view. *International Geology Review* 41, 1114–1124.
- Li, Z.X., Li, X.H., Kinny, P.D., Wang, J., Zhang, S., Zhou, H., 2003. Geochronology of Neoproterozoic syn-rift magmatism in the Yangtze Craton, South China and correlations with other continents: evidence for a mantle superplume that broke up Rodinia. *Precambrian Research* 122, 85–109.
- Li, X.H., Qi, C., Liu, Y., 2005. Rapid separation of Hf from rock samples for isotope analysis by MC-ICPMS: a modified single-column extraction chromatography method. *Geochimica (in Chinese with English abstract)* 34, 109–114.
- Liu, C.Q., Masuda, A., Xie, G.H., 1994. Major- and trace-element compositions of Cenozoic basalts in eastern China: Petrogenesis and mantle source. *Chemical Geology* 114, 19–42.
- Liu, Y.S., Gao, S., Yuan, H.L., Zhou, L., Liu, X.M., Wang, X.C., Hu, Z.C., Wang, L.S., 2004. U–Pb zircon ages and Nd, Sr, and Pb isotopes of lower crustal xenoliths from North China Craton: insights on evolution of lower continental crust. *Chemical Geology* 211, 87–109.
- Liu, D.Y., Jian, P., Kröner, A., Xu, S.T., 2006a. Dating of prograde metamorphic events deciphered from episodic zircon growth in rocks of the Dabie–Sulu UHP complex, China. *Earth and Planetary Science Letters* 250, 650–666.
- Liu, F.L., Gerdes, A., Liou, J.G., Xue, H.M., Liang, F.H., 2006b. SHRIMP U–Pb zircon dating from Sulu–Dabie dolomitic marble, South China: constraints on prograde, ultrahigh-pressure and retrograde metamorphic ages. *Journal of Metamorphic Geology* 24, 569–589.
- Liu, Y.S., Gao, S., Kelemen, P.B., Xu, W.L., 2008. Recycled crust controls contrasting source compositions of Mesozoic and Cenozoic basalts in the North China Craton. *Geochimica et Cosmochimica Acta* 72, 2349–2376.
- Lustrino, M., 2005. How the delamination and detachment of lower crust can influence basaltic magmatism. *Earth-Science Reviews* 72, 21–38.
- Ma, X.Y., Wu, D.N., 1987. Cenozoic extensional tectonics in China. *Tectonophysics* 133, 243–255.
- McDonough, W.F., Sun, S.-S., 1995. The composition of the Earth. *Chemical Geology* 120, 223–253.
- McKenzie, D., Bickle, M.J., 1988. The volume and composition of melt generated by extension of the lithosphere. *Journal of Petrology* 29, 625–679.
- Menzies, M.A., Fan, W., Ming, Z., 1993. Palaeozoic and Cenozoic lithoprobes and loss of > 120 km of Archaean lithosphere, Sino–Korean craton, China. In: Prichard, H.M., Alabaster, T., Harris, N.B.W., Neary, C.R. (Eds.), *Magmatic Processes and Plate Tectonics*. Geological Society Special Publication, vol. 76, pp. 71–81.
- Menzies, M., Xu, Y.G., Zhang, H.F., Fan, W.M., 2007. Integration of geology, geophysics and geochemistry: a key to understanding the North China Craton. *Lithos* 96, 1–21.
- Muenker, C., Weyer, S., Scherer, E., Mezger, K., 2001. Separation of high field strength elements (Nb, Ta, Zr, Hf) and Lu from rock samples for MC-ICPMS measurements. *Geochemistry Geophysics Geosystems* 2 No. 2001GC000183.
- Niu, Y.L., 2005. Generation and evolution of basaltic magmas: some basic concepts and a new view on the origin of Mesozoic–Cenozoic basaltic volcanism in Eastern China. *Geological Journal of China Universities* 11, 1–38.
- Niu, Y.L., O'Hara, M.J., 2003. Origin of ocean island basalts: a new perspective from petrology, geochemistry, and mineral physics considerations. *Journal of Geophysical Research* 108, B4 (2209). doi:10.1029/2002JB002048.
- Pearson, D.G., Wittig, N., 2008. Formation of Archaean continental lithosphere and its diamonds: the root of the problem. *Journal of the Geological Society* 165, 895–914.
- Peng, Z.C., Zartman, R.E., Futa, K., Chen, D.G., 1986. Pb-, Sr- and Nd-isotopic systematics and chemical characteristics of Cenozoic basalts, eastern China. *Chemical Geology* 59, 3–33.

- Pertermann, M., Hirschmann, M.M., 2003. Partial melting experiments on a MORB-like pyroxenite between 2 and 3 GPa; constraints on the presence of pyroxenite in basalt source regions from solidus location and melting rate. *Journal of Geophysical Research* 108 (B2), 2125. doi:10.1029/2000JB000118.
- Plank, T., Langmuir, C.H., 1998. The chemical composition of subducting sediment and its consequences for the crust and mantle. *Chemical Geology* 145, 325–394.
- Qi, Q., Taylor, L.A., Zhou, X.M., 1994. Geochemistry and petrogenesis of three series of Cenozoic basalts from southeastern China. *International Geology Review* 36, 435–451.
- Rapp, R.P., Watson, E.B., Miller, C.F., 1991. Partial melting of amphibolite/eclogite and the origin of Archean trondhjemites and tonalites. *Precambrian Research* 51, 1–25.
- Rapp, R.P., Shimizu, N., Norman, M.D., Applegate, G.S., 1999. Reaction between slab-derived melts and peridotite in the mantle wedge: experimental constraints at 3.8 GPa. *Chemical Geology* 160, 335–356.
- Rapp, R.P., Shimizu, N., Norman, M.D., 2003. Growth of early continental crust by partial melting of eclogite. *Nature* 425, 605–609.
- Reisberg, L., Zhi, X.C., Lorand, J.-P., Wagner, C., Peng, Z.C., Zimmermann, C., 2005. Re–Os and S systematics of spinel peridotite xenoliths from east central China: evidence for contrasting effects of melt percolation. *Earth and Planetary Science Letters* 239, 286–308.
- Richards, M.A., Duncan, R.A., Courtillot, V.E., 1989. Flood basalts and hot-spot tracks: plume heads and tails. *Science* 246, 103–107.
- Rudnick, R.L., Barth, M., Horn, I., McDonough, W.F., 2000. Rutile-bearing refractory eclogites: missing link between continents and depleted mantle. *Science* 287, 278–281.
- Rudnick, R.L., Gao, S., Ling, W.L., Liu, Y.-s., McDonough, W.F., 2004. Petrology and geochemistry of spinel peridotite xenoliths from Hannuoba and Qixia, North China Craton. *Lithos* 77, 609–637.
- Rumble, D., Giorgis, D., Orelund, T., Zhang, Z.M., Xu, H.F., Yui, T.F., Yang, J.S., Xu, Z.Q., Liou, J.G., 2002. Low  $\delta^{18}\text{O}$  zircons, U–Pb dating, and the age of the Qinglongshan oxygen and hydrogen isotope anomaly near Donghai in Jiangsu province, China. *Geochimica et Cosmochimica Acta* 66, 2299–2306.
- Silver, P.G., Behn, M.D., Kelley, K., Schmitz, M., Savage, B., 2006. Understanding cratonic flood basalts. *Earth and Planetary Science Letters* 245, 190–201.
- Smith, A., 1998. The geodynamic significance of the Dupal anomaly in Asia. In: Flower, M.F.J., Chung, S.-L., Lo, C.-H., Lee, T.-Y. (Eds.), *Mantle Dynamics and Plate Interactions in East Asia*. American Geophysical Union Geodynamics Series, vol. 27, pp. 89–105.
- Sobolev, A.V., Hofmann, A.W., Sobolev, S.V., Nikogosian, I.K., 2005. An olivine-free mantle source of Hawaiian shield basalts. *Nature* 434, 590–597.
- Sobolev, A.V., Hofmann, A.W., Kuzmin, D.V., Yaxley, G.M., Arndt, N.T., Chung, S.-L., Danyushevsky, L.V., Elliott, T., Frey, F.A., Garcia, M.O., Gurenko, A.A., Kamenetsky, V.S., Kerr, A.C., Krivolutskaia, N.A., Matvienkov, V.V., Nikogosian, I.K., Rocholl, A., Sigurdsson, I.A., Sushchevskaya, N.M., Tekley, M., 2007. The amount of recycled crust in sources of mantle-derived melts. *Science* 316, 412–417.
- Song, Y., Frey, F.A., Zhi, X., 1990. Isotopic characteristics of Hannuoba basalts, eastern China: Implications for their petrogenesis and the composition of subcontinental mantle. *Chemical Geology* 88, 35–52.
- Sorensen, S.S., Grossman, J.N., 1993. Accessory minerals and subduction zone metasomatism: a geochemical comparison of two mélanges (Washington and California, U.S.A.). *Chemical Geology* 110, 269–297.
- Sun, S.-S., McDonough, W.F., 1989. Chemical and isotopic systematics of oceanic basalts: implications for mantle composition and processes. *Geological Society Special Publications* 42, 313–345.
- Sun, W.D., Ding, X., Hu, Y.-H., Li, X.-H., 2007. The golden transformation of the Cretaceous plate subduction in the west Pacific. *Earth and Planetary Science Letters* 262, 533–542.
- Takahashi, E., Kushiro, I., 1983. Melting of a dry peridotite at high pressures and basalt magma genesis. *American Mineralogist* 68, 859–879.
- Tang, Y.-J., Zhang, H.-F., Ying, J.-F., 2006. Asthenosphere–lithospheric mantle interaction in an extensional regime: implication from the geochemistry of Cenozoic basalts from Taihang Mountains, North China Craton. *Chemical Geology* 233, 309–327.
- Tang, J., Zheng, Y.-F., Wu, Y.-B., Gong, B., Zha, X.P., Liu, X.-M., 2008a. Zircon U–Pb age and geochemical constraints on the tectonic affinity of the Jiaodong terrane in the Sulu orogen, China. *Precambrian Research* 161, 389–418.
- Tang, J., Zheng, Y.-F., Gong, B., Wu, Y.-B., Gao, T.-S., Yuan, H.L., Wu, F.-Y., 2008b. Extreme oxygen isotope signature of meteoric water in magmatic zircon from metagranite in the Sulu orogen, China: implications for Neoproterozoic rift magmatism. *Geochimica et Cosmochimica Acta* 72, 3139–3169.
- Tatsumi, Y., Eggins, S., 1995. *Subduction Zone Magmatism*. Blackwell Science, Oxford, 211 pp.
- Tian, Z.Y., 1990. The formation and distribution of Mesozoic–Cenozoic sedimentary basins in China. *Journal of Petrology and Geology* 13, 19–34.
- Valley, J.W., Kitchen, N., Kohn, M.J., Niendorf, C.R., Spicuzza, M.J., 1995. UWG-2, a garnet standard for oxygen isotope ratio: strategies for high precision and accuracy with laser heating. *Geochimica et Cosmochimica Acta* 59, 5223–5231.
- Valley, J.W., Kinny, P.D., Schulze, D.J., Spicuzza, M.J., 1998. Zircon megacrysts from kimberlite: oxygen isotope variability among mantle melts. *Contributions to Mineralogy and Petrology* 133, 1–11.
- van Westrenen, W., Blundy, J.D., Wood, B.J., 2000. Effect of  $\text{Fe}^{2+}$  on garnet–melt trace element partitioning: experiments in FCMS and quantification of crystal–chemical controls in natural systems. *Lithos* 53, 189–201.
- Wagner, T.P., Grove, T.L., 1998. Melt/harzburgite reaction in the petrogenesis of tholeiitic magma from Kilauea volcano, Hawaii. *Contributions to Mineralogy and Petrology* 131, 1–12.
- Walter, M.J., 1998. Melting of garnet peridotite and the origin of komatiite and depleted lithosphere. *Journal of Petrology* 39, 29–60.
- Wang, Z.R., Kitchen, N.E., Eiler, J.M., 2003. Oxygen isotope geochemistry of the second HSDP core. *Geochemistry Geophysics Geosystems* 4 No. 8712.
- Watson, M.P., Hayward, A.B., Parkinson, D.N., Zhang, Z.H., 1987. Plate tectonic history, basin development and petroleum source rock deposition onshore China. *Marine and Petroleum Geology* 4, 205–225.
- White, R.S., McKenzie, D., 1989. Magmatism at rift zones: the generation of volcanic continental margins and flood basalts. *Journal of Geophysical Research* B94, 7685–7729.
- White, R.S., McKenzie, D., 1995. Mantle plumes and flood basalts. *Journal of Geophysical Research* B100, 7543–7585.
- Wilde, S.A., Zhou, X.H., Nemchin, A.A., Sun, M., 2003. Mesozoic crust–mantle interaction beneath the North China craton: a consequence of the dispersal of Gondwanaland and accretion of Asia. *Geology* 31, 817–820.
- Wu, F.Y., Walker, R.J., Ren, X.W., Sun, D.Y., Zhou, X.H., 2003. Osmium isotopic constraints on the age of lithospheric mantle beneath northeastern China. *Chemical Geology* 197, 107–129.
- Wu, F.Y., Lin, J.Q., Wilde, S.A., Zhang, X.O., Yang, J.H., 2005. Nature and significance of the Early Cretaceous giant igneous event in eastern China. *Earth and Planetary Science Letters* 233, 103–119.
- Wu, Y.-B., Zheng, Y.-F., Zhao, Z.-F., Gong, B., Liu, X.M., Wu, F.-Y., 2006. U–Pb, Hf and O isotope evidence for two episodes of fluid-assisted zircon growth in marble-hosted eclogites from the Dabie orogen. *Geochimica et Cosmochimica Acta* 70, 3743–3761.
- Wu, Y.-B., Zheng, Y.-F., Tang, J., Gong, B., Zhao, Z.-F., Liu, X.M., 2007. Zircon U–Pb dating of water–rock interaction during Neoproterozoic rift magmatism in South China. *Chemical Geology* 246, 65–86.
- Xiong, X.L., Adam, T.J., Green, T.H., 2005. Rutile stability and rutile/melt HFSE partitioning during partial melting of hydrous basalt: implications for TTG genesis. *Chemical Geology* 218, 339–359.
- Xu, Y.G., 2001. Thermo-tectonic destruction of the Archaean lithospheric keel beneath the Sino-Korean craton in China: evidence, timing and mechanism. *Physics and Chemistry of the Earth (A)* 26, 747–757.
- Xu, Y.G., Bodinier, J.-L., 2004. Contrasting enrichments in high and low temperature xenoliths from Nushan, Eastern China: results of a single metasomatic event during lithospheric accretion? *Journal of Petrology* 45, 321–341.
- Xu, Y.G., Chung, S.-L., Ma, J., Shi, L., 2004. Contrasting Cenozoic lithospheric evolution and architecture in western and eastern Sino-Korean Craton: constraints from geochemistry of basalts and mantle xenoliths. *The Journal of Geology* 112, 593–605.
- Xu, Y.G., Ma, J.L., Frey, F.A., Feigenson, M.D., Liu, J.F., 2005. Role of lithosphere–asthenosphere interaction in the genesis of Quaternary alkalic and tholeiitic basalts from Datong, western North China Craton. *Chemical Geology* 224, 247–271.
- Xu, X.S., Griffin, W.L., O'Reilly, S.Y., Pearson, N.J., Geng, H.Y., Zheng, J.P., 2008. Re–Os isotopes of sulfides in mantle xenoliths from eastern China: progressive modification of lithospheric mantle. *Lithos* 102, 43–64.
- Yang, H.-J., Frey, F.A., Clague, D.A., 2003. Constraints on the source components of lavas forming the Hawaiian North Arch and Honolulu volcanics. *Journal of Petrology* 44, 603–627.
- Yaxley, G.M., 2000. Experimental study of the phase and melting relations of homogeneous basalt + peridotite mixtures and implications for the petrogenesis of flood basalts. *Contributions to Mineralogy and Petrology* 139, 326–338.
- Yaxley, G.M., Green, D.H., 1998. Reactions between eclogite and peridotite: mantle refertilisation by subduction of oceanic crust. *Schweizerische Mineralogische et Petrologische Mitteilungen* 78, 243–255.
- Ying, J.F., Zhang, H.F., Kita, N., Morishita, X.H., Shimoda, G., 2006. Nature and evolution of Late Cretaceous lithospheric mantle beneath the eastern North China Craton: constraints from petrology and geochemistry of peridotitic xenoliths from Jünan, Shandong Province, China. *Earth and Planetary Science Letters* 244, 622–638.
- Yu, J.H., Xu, X.S., O'Reilly, S.Y., Griffin, W.L., Zhang, M., 2003. Granulite xenoliths from Cenozoic Basalts in SE China provide geochemical fingerprints to distinguish lower crust terranes from the North and South China tectonic blocks. *Lithos* 67, 77–102.
- Yuan, H.L., Gao, S., Rudnick, R.L., Jin, Z.M., Liu, Y.S., Puchtel, I.S., Walker, R.J., Yu, R.D., 2007. Re–Os evidence for the age and origin of peridotites from the Dabie–Sulu ultrahigh pressure metamorphic belt, China. *Chemical Geology* 236, 323–338.
- Zhang, H.F., Sun, M., Zhou, X.H., Zhou, M.F., Fan, W.M., Zheng, J.P., 2003. Secular evolution of the lithosphere beneath the eastern North China Craton: evidence from Mesozoic basalts and high–Mg andesites. *Geochimica et Cosmochimica Acta* 67, 4373–4387.
- Zhang, H.-F., Goldstein, S.L., Zhou, X.-H., Sun, M., Zheng, J.-P., Cai, Y., 2008. Evolution of subcontinental lithospheric mantle beneath eastern China: Re–Os isotopic evidence from mantle xenoliths in Paleozoic kimberlites and Mesozoic basalt. *Contributions to Mineralogy and Petrology* 157, 271–293.
- Zhao, Z.-F., Zheng, Y.-F., Wei, C.-S., Wu, Y.-B., 2007. Post-collisional granitoids from the Dabie orogen in China: Zircon U–Pb age, element and O isotope evidence for recycling of subducted continental crust. *Lithos* 93, 248–272.
- Zheng, Y.-F., 1993. Calculation of oxygen isotope fractionation in anhydrous silicates. *Geochimica et Cosmochimica Acta* 55, 2299–2307.
- Zheng, Y.-F., 2008. A perspective view on ultrahigh-pressure metamorphism and continental collision in the Dabie–Sulu orogenic belt. *Chinese Science Bulletin* 53, 3081–3104.
- Zheng, Y.-F., Fu, B., 1998. Estimation of oxygen diffusivity from anion porosity in minerals. *Geochemical Journal* 32, 71–89.
- Zheng, Y.-F., Zhang, S.-B., 2007. Formation and evolution of Precambrian continental crust in South China. *Chinese Science Bulletin* 52, 1–12.
- Zheng, Y.-F., Fu, B., Li, Y., Xiao, Y., Li, S., 1998. Oxygen and hydrogen isotope geochemistry of ultrahigh-pressure eclogites from the Dabie Mountains and the Sulu terrane. *Earth and Planetary Science Letters* 155, 113–129.
- Zheng, J.P., O'Reilly, S.Y., Griffin, W.L., Lu, F.X., Zhang, M., Pearson, N.J., 2001. Relict refractory mantle beneath the eastern North China block: significance for lithosphere evolution. *Lithos* 57, 43–66.

- Zheng, Y.-F., Wang, Z.R., Li, S.G., Zhao, Z.F., 2002. Oxygen isotope equilibrium between eclogite minerals and its constraints on mineral Sm–Nd chronometer. *Geochimica et Cosmochimica Acta* 66, 625–634.
- Zheng, Y.-F., Fu, B., Gong, B., Li, L., 2003. Stable isotope geochemistry of ultrahigh pressure metamorphic rocks from the Dabie–Sulu orogen in China: implications for geodynamics and fluid regime. *Earth-Science Reviews* 62, 105–161.
- Zheng, Y.-F., Wu, Y.B., Chen, F.-K., Gong, B., Li, L., Zhao, Z.F., 2004. Zircon U–Pb and oxygen isotope evidence for a large-scale  $^{18}\text{O}$  depletion event in igneous rocks during the Neoproterozoic. *Geochimica et Cosmochimica Acta* 68, 4145–4165.
- Zheng, Y.-F., Zhou, J.-B., Wu, Y.-B., Zhao, Z.-F., 2005. Low-grade metamorphic rocks in the Dabie–Sulu orogenic belt: a passive-margin accretionary wedge deformed during continent subduction. *International Geology Review* 47, 851–871.
- Zheng, Y.-F., Zhao, Z.-F., Wu, Y.-B., Zhang, S.-B., Liu, X.M., Wu, F.-Y., 2006. Zircon U–Pb age, Hf and O isotope constraints on protolith origin of ultrahigh-pressure eclogite and gneiss in the Dabie orogen. *Chemical Geology* 231, 135–158.
- Zheng, Y.-F., Wu, Y.-B., Gong, B., Chen, R.-X., Tang, J., Zhao, Z.-F., 2007. Tectonic driving of Neoproterozoic glaciations: evidence from extreme oxygen isotope signature of meteoric water in granite. *Earth and Planetary Science Letters* 256, 196–210.
- Zhi, X.C., Song, Y., Frey, F.A., Feng, J., Zhai, M., 1990. Geochemistry of Hannuoba basalts, eastern China: constraints on the origin of continental alkalic and tholeiitic basalt. *Chemical Geology* 88, 1–33.
- Zhou, X.H., Armstrong, R.L., 1982. Cenozoic volcanic rocks of eastern China, secular and geographic trends in chemistry and strontium isotopic composition. *Earth and Planetary Science Letters* 58, 301–329.
- Zhou, X.H., Zhu, B.Q., Liu, R.X., Chen, W.J., 1988. Cenozoic basaltic rocks in Eastern China. *Continental Flood Basalts*. Kluwer Academic Publishers, Dordrecht. 311–330 pp.
- Zindler, A., Hart, S., 1986. Chemical geodynamics. *Annual Review on Earth and Planetary Sciences* 14, 493–571.
- Zou, H., Zindler, A., Xu Xisheng, Qi, Q., 2000. Major, trace element, and Nd, Sr and Pb isotope studies of Cenozoic basalts in SE China; mantle sources, regional variations, and tectonic significance. *Chemical Geology* 171, 33–47.